

## Mass Transfer in Eccentric Orbits with Self-consistent Stellar Evolution

KYLE AKIRA ROCHA,<sup>1,2,3</sup> RACHEL HUR,<sup>1,4</sup> VICKY KALOGERA,<sup>1,2,3</sup> SETH GOSSAGE,<sup>1,3</sup> MENG SUN,<sup>1</sup> ZOHEYR DOCTOR,<sup>1</sup>  
JEFF J. ANDREWS,<sup>5,6</sup> SIMONE S. BAVERA,<sup>7,8</sup> MAX BRIEL,<sup>7,8</sup> TASSOS FRAGOS,<sup>7,8</sup> KONSTANTINOS KOVLAKAS,<sup>9,10</sup>  
MATTHIAS U. KRUCKOW,<sup>7,8</sup> DEVINA MISRA,<sup>7,11</sup> ZEPEI XING,<sup>7,8</sup> AND EMMANOUIL ZAPARTAS<sup>12,13</sup>

<sup>1</sup>*Center for Interdisciplinary Exploration and Research in Astrophysics (CIERA), 1800 Sherman, Evanston, IL 60201, USA*

<sup>2</sup>*Department of Physics & Astronomy, Northwestern University, 2145 Sheridan Road, Evanston, IL 60208, USA*

<sup>3</sup>*NSF-Simons AI Institute for the Sky (SkAI), 172 E. Chestnut St., Chicago, IL 60611, USA*

<sup>4</sup>*The Department of Physics, 5720 South Ellis Avenue, Chicago, IL 60637*

<sup>5</sup>*Department of Physics, University of Florida, 2001 Museum Rd, Gainesville, FL 32611, USA*

<sup>6</sup>*Institute for Fundamental Theory, 2001 Museum Rd, Gainesville, FL 32611, USA*

<sup>7</sup>*Département d'Astronomie, Université de Genève, Chemin Pegasi 51, CH-1290 Versoix, Switzerland*

<sup>8</sup>*Gravitational Wave Science Center (GWSC), Université de Genève, CH1211 Geneva, Switzerland*

<sup>9</sup>*Institute of Space Sciences (ICE, CSIC), Campus UAB, Carrer de Magrans, 08193 Barcelona, Spain*

<sup>10</sup>*Institut d'Estudis Espacials de Catalunya (IEEC), Carrer Gran Capità, 08034 Barcelona, Spain*

<sup>11</sup>*Institutt for Fysikk, Norwegian University of Science and Technology, Trondheim, Norway*

<sup>12</sup>*Institute of Astrophysics, FORTH, N. Plastira 100, Heraklion, 70013, Greece*

<sup>13</sup>*IAASARS, National Observatory of Athens, Vas. Pavlou and I. Metaxa, Penteli, 15236, Greece*

### ABSTRACT

We investigate Roche lobe overflow mass transfer (MT) in eccentric binary systems between stars and compact objects (COs), modeling the coupled evolution of both the star and the orbit due to eccentric MT (eMT) in a self-consistent framework. We implement the analytic expressions for secular rates of change of the orbital semi-major axis and eccentricity, assuming a delta function MT at periaapse, into the binary stellar evolution code **MESA**. Two scenarios are examined: (1) a simplified model isolating the effects of eMT on stellar and orbital evolution, and (2) realistic binary configurations that include angular momentum exchange (e.g., tides, mass loss, spin-orbit coupling, and gravitational wave radiation). Unlike the ad hoc approach of instant circularization that is often employed, explicit modeling of eMT reveals a large fraction of binaries can remain eccentric post-MT. Even binaries which naturally circularize during eMT have different properties (donor mass and orbital size) compared to predictions from instant circularization, with some showing fundamentally different evolutionary outcomes (e.g., stable versus unstable MT). We demonstrate that a binary's initial mass ratio and eccentricity are predictive of whether it will remain eccentric or circularize after eMT. These findings underscore the importance of eMT in understanding CO-hosting binary populations, including X-ray binaries, gravitational wave sources, and other high-energy transients.

*Keywords:* Astronomical simulations (1857); Binary stars (154); Close binary stars (254); Compact binary stars (283); Interacting binary stars (801); Compact objects (288); Black holes (162); Neutron stars (1108); Gravitational wave sources (677); Stellar evolutionary models (2046); Stellar populations (1622)

### 1. INTRODUCTION

Binary stellar interactions produce a wide array of high-energy astrophysical phenomena, including supernova explosions, X-ray binaries (XRBs), gravitational

wave (GW) sources, and exotic stellar objects such as blue stragglers, hot subdwarfs and barium stars (for reviews see; e.g., Baily 1995; Heber 2009; Langer 2012; Tauris & van den Heuvel 2023; Marchant & Bodensteiner 2024; Wang & Ryu 2024). Primary among these interactions is mass transfer (MT) via Roche-lobe overflow (RLO), which has long been understood as integral

in determining the evolution and ultimate fate of binary systems (Kuiper 1941; Paczyński 1971; Eggleton 1983; Webbink 1984). The exchange of energy and angular momentum during RLO MT drives orbital evolution, producing a plethora of complex evolutionary sequences and phenomena (e.g., Lubow & Shu 1975; Kolb & Ritter 1990). It is through this lenses that we interpret Low- and High-mass XRBs (e.g., Bahramian & Degenaar 2023; Kretschmar et al. 2019; Fornasini et al. 2023), binary compact object (CO) mergers detected by the LIGO-Virgo-KAGRA collaboration (Abbott et al. 2023), transients such as supernovae with evidence for circumstellar interaction (e.g., Moriya et al. 2015; Zhu et al. 2024), wide binaries hosting quiescent COs discovered with Gaia (e.g., Andrews et al. 2022; El-Badry et al. 2022, 2023a,b; Gaia Collaboration et al. 2024), and gravitation wave sources which will be detectable by the Laser Interferometer Space Antenna (LISA) mission (e.g., Lamberts et al. 2019; Tang et al. 2024). Although extensively studied for over five decades, numerical models for binary evolution due to RLO MT have primarily considered circular orbits, neglecting eccentricity, a fundamental orbital property for many binary systems observed in nature.

Eccentric orbits are abundantly observed in both pre- and post-MT binary systems; understanding how eccentric orbits may evolve through RLO MT is then paramount to understanding the nature of such systems. During main sequence (MS) evolution, many binaries are observed to have significantly eccentric orbits, which may provide both clues to their formation mechanisms and have consequences for their future evolution (Mathieu 1994; Geller et al. 2019; Muñoz & Lithwick 2020; D’Orazio & Duffell 2021; Hwang et al. 2022; Lubow 2022; Bashi et al. 2023; Lai & Muñoz 2023; Siwek et al. 2023; Hu et al. 2024). Just prior to the onset of MT, ellipsoidal variables in the Large Magellanic Clouds retain significant eccentricity, in tension with standard tidal theory (e.g., Nie et al. 2017). High-mass X-ray binaries (HMXBs) hosting COs are observed in eccentric orbits (e.g., Raguzova & Popov 2005; Neumann et al. 2023; Fortin et al. 2023) and are expected to evolve into RLO MT when the donor leaves the MS evolution while still eccentric (van den Heuvel 2019). Finally, post-MT binaries hosting blue stragglers, barium, S-type stars and some post-AGB systems are observed to be in eccentric orbits (e.g., Geller et al. 2009; Milliman et al. 2014; Gosnell et al. 2015; Milliman et al. 2016; Van der Swaelmen et al. 2017; Oomen et al. 2018; Geller et al. 2021; Escorza & De Rosa 2023; Nine et al. 2024; Linck et al. 2024), suggesting that a number of systems may gain or retain their eccentricity through RLO MT.

Although well motivated by observations, eccentric RLO MT is not trivially implemented into standard binary evolution calculations due to: (i) the commonly adopted Roche lobe model used to determine MT conditions (Eggleton 1983; Ritter 1988; Kolb & Ritter 1990) may not apply in an eccentric orbit, as the resulting MT interactions may require adoption of results from hydrodynamical simulations (e.g. non-conservative MT and re-accretion; Lajoie & Sills 2011; Saladino & Pols 2019), (ii) the quantitative effects of RLO MT events on the long-term (secular) orbital evolution are challenging to calculate, depend on assumptions for MT conditions along the orbit, and analytical expressions are needed for population studies (e.g., Sepinsky et al. 2007b, 2009; Dosopoulou & Kalogera 2016; Hamers & Dosopoulou 2019, and references therein). Therefore, in detailed binary evolution simulations eccentricity is often not accounted for in MT phases. Instead, binary orbits are either assumed to be circular at the Zero Age Main Sequence (ZAMS) of the binary system or, if later in the evolution MT is encountered (at periape) for eccentric binaries, then an ad hoc assumption of instantaneous circularization is made (e.g., Hurley et al. 2002; Naoz et al. 2016; Ivanova et al. 2005; Eldridge et al. 2017; Giacobbo et al. 2018; Sun & Arras 2018; Breivik et al. 2020; Marchant et al. 2021; Sun et al. 2021; Rodriguez et al. 2022; Fragos et al. 2023; Simaz Bunzel et al. 2023; Sun & Mathieu 2023; Andrews et al. 2024; Sun et al. 2024, and others).

In this work, we model the secular effects of eccentric mass transfer (eMT) on binary orbital evolution, using the 1D stellar evolution code Modules for Experiments in Stellar Astrophysics (MESA, version 11701) (Paxton et al. 2011, 2015, 2013, 2018, 2019) along with the MESA software development kit (version 20190503) (Townsend 2020). We also include other factors that impact mass and angular momentum evolution, such as tides, stellar winds, magnetic braking, and gravitational waves. Previous theoretical work involved deriving the proper secular effects of RLO MT in eccentric binary systems without the simultaneous evolution of the stellar companion (e.g., Sepinsky et al. 2007b; Hamers & Dosopoulou 2019). We expand on this work, modeling the simultaneous evolution of both the star and orbit due to eMT.

In Section 2 we detail our choices for orbital evolution due to eccentric MT and implementation into MESA. In Section 3 we present a small parameter study with simplified models, to isolate the effects of eccentric MT. In Section 4 we present our fiducial eccentric MT models with astrophysical initial conditions. Finally, in Section 5 we discuss our findings and summarize with concluding remarks.

## 2. METHODS

### 2.1. Treatment of Eccentric Mass Transfer

We consider a binary with primary mass  $M_1$ , a secondary mass  $M_2$ , an orbital semi-major axis  $a$ , and an eccentricity  $e$ . The total orbital angular momentum,  $J_{\text{orb}}$ , is:

$$J_{\text{orb}} = M_1 M_2 \sqrt{\frac{Ga(1-e^2)}{M_1 + M_2}}, \quad (1)$$

where  $G$  is the gravitational constant. The binary orbital period,  $P_{\text{orb}}$ , is related to the semi-major through Kepler's third law. The time derivative of Equation 1 can be written as:

$$\frac{\dot{J}_{\text{orb}}}{J_{\text{orb}}} = \frac{\dot{M}_1}{M_1} + \frac{\dot{M}_2}{M_2} - \frac{1}{2} \frac{\dot{M}_1 + \dot{M}_2}{M_1 + M_2} + \frac{1}{2} \frac{\dot{a}}{a} - \frac{e\dot{e}}{1-e^2}. \quad (2)$$

In the classical case of a circular orbit with fully conservative RLO MT (where all transferred mass is accreted), the total mass is conserved with  $\dot{M}_2 = -\dot{M}_1$ , and the total orbital angular momentum is conserved, with  $\dot{J}_{\text{orb}} = 0$ . Then, Equation 2 can be solved explicitly for the rate of change in the semi-major axis:  $\dot{a} = 2a(q-1)\frac{\dot{M}_1}{M_1}$ , where we define  $q = M_1/M_2$  as the mass ratio. As expected, the orbit shrinks when  $q > 1$  and expands when  $q < 1$ .

In the case of an eccentric orbit, more complex methods are required to derive expressions for the secular rate of change of orbital elements  $\dot{a}$  and  $\dot{e}$ . Such derivations have been carried out using variations of different formalisms (e.g., Sepinsky et al. 2007b, 2009, 2010; Dosopoulou & Kalogera 2016; Hamers & Dosopoulou 2019, and references therein). In this study, we incorporate the formalism from Sepinsky et al. 2009 which is only analytical treatment currently available that can account for non-conservative MT and can be applied to large-scale detailed binary evolution simulations.

We adopt Equations (18) and (19) from Sepinsky et al. (2009) which provide the secular rates of change for the semi-major axis  $a$  and eccentricity  $e$  as follows:

$$\begin{aligned} \left\langle \frac{da}{dt} \right\rangle_{\text{sec}} &= \frac{a \dot{M}_0}{\pi M_1} \frac{1}{(1-e^2)^{1/2}} \\ &\times \left[ e \frac{|\vec{r}_{A_1, P}|}{a} + \gamma q e \frac{|\vec{r}_{A_2}|}{a} \cos \Phi_P \right. \\ &+ (\gamma q - 1)(1 - e^2) \\ &\left. + (1 - \gamma) \left( \mu + \frac{1}{2} \right) (1 - e^2) \frac{q}{q + 1} \right], \quad (3) \end{aligned}$$

$$\begin{aligned} \left\langle \frac{de}{dt} \right\rangle_{\text{sec}} &= \frac{(1-e^2)^{1/2} \dot{M}_0}{2\pi M_1} \\ &\times \left[ \gamma q \frac{|\vec{r}_{A_2}|}{a} \cos \Phi_P + \frac{|\vec{r}_{A_1, P}|}{a} \right. \\ &+ 2(\gamma q - 1)(1 - e) \\ &\left. + 2(1 - \gamma) \left( \mu + \frac{1}{2} \right) (1 - e) \frac{q}{q + 1} \right], \quad (4) \end{aligned}$$

these equations can account for non-conservative MT, where  $\gamma = 1 - \beta$  is the fraction of mass transferred through RLO that is accreted by the secondary ( $\dot{M}_2 = -\gamma \dot{M}_1$ );  $A_1$  is the location where mass is lost from the donor at the  $L_1$  point;  $A_2$  is the point on the accretor where mass is accreted;  $\vec{r}_{A_1}$  and  $\vec{r}_{A_2}$  are the position vectors of  $A_1$  and  $A_2$  relative to the centers of mass of the donor and accretor, respectively;  $\Phi$  is the angle between the line connecting both component stars and the vector  $\vec{r}_{A_2}$ ; and subscript  $P$  denotes a quantity is taken at periape. Then,  $\mu$  parametrizes the specific orbital angular momentum of material lost during non-conservative MT which we take to be the specific orbital angular momentum of the accretor ( $\mu = q$ ). We refer the reader to Figure 1 in Sepinsky et al. 2007b for definitions of all quantities listed here. Hereafter, Equations 3 and 4 will be denoted  $\dot{a}_{\text{eMT}}$  and  $\dot{e}_{\text{eMT}}$  respectively.

In this study, we model CO accretors for which we assume  $\vec{r}_{A_2}/a \ll 1$  which implicitly accounts for  $\Phi_P$ , following the simplified cases described in Sepinsky et al. 2007b. Instead of assuming the star is exactly Roche-filling at all times during MT, we explicitly calculate the MT rate (Section 2.3.1). The MT efficiency  $\gamma$  is assumed to be conservative up to the Eddington limit which is also explicitly calculated during evolution (Section 2.3).

The advantage of these secular evolution equations is that they are analytical while also accounting for non-conservative MT, and they are derived under the following simplifying assumption: RLO MT occurs as a delta function at periape with a MT rate  $\dot{M}_1 = \dot{M}_0 \delta(v)$ , where  $\dot{M}_0$  is the instantaneous MT rate,  $\delta$  is the Dirac delta function, and  $v$  is the true anomaly. For a complete derivation and a list of all assumptions and their implications, we refer the reader to Sepinsky et al. 2007b, 2009. We note that while Hamers & Dosopoulou 2019 extend beyond the delta function MT approximation with a phase dependent MT rate, their formalism is limited to conservative RLO MT only. Therefore, we use the equations by Sepinsky et al. 2009, as many binary systems are expected to undergo phases of non-conservative MT which significantly impacts their evolution (e.g., Marino et al. 2017; Ziłkowski & Zdziarski 2018).

### 2.2. Implementation in MESA

We incorporate the equations of secular orbital evolution due to eccentric MT into MESA by combining individual sinks (e.g. mass loss) and sources (e.g. mass accretion) of angular momentum transport. These are assumed to be decoupled, such that  $\dot{J}_{\text{orb}}$  can be determined by a linear combination of individual effects (Paxton et al. 2015):

$$\dot{J}_{\text{orb}} = \dot{J}_{\text{gr}} + \dot{J}_{\text{ml}} + \dot{J}_{\text{mb}} + \dot{J}_{\text{ls}}, \quad (5)$$

where subscripts denote angular momentum changes due to gravitational wave radiation ( $\dot{J}_{\text{gr}}$ ), mass loss ( $\dot{J}_{\text{ml}}$ ), magnetic braking ( $\dot{J}_{\text{mb}}$ ), and spin-orbit coupling ( $\dot{J}_{\text{ls}}$ ). Within  $\dot{J}_{\text{ml}}$ , are contributions from circular non-conservative RLO MT and wind mass loss. We replace the contribution from circular non-conservative RLO MT, with the contribution from eccentric MT by reparameterizing  $\dot{a}_{\text{eMT}}$  and  $\dot{e}_{\text{eMT}}$  in terms of the orbital angular momentum via Equation 2.

Similar to Equation 5, we calculate the rate of change of orbital eccentricity,  $\dot{e}_{\text{orb}}$ , as a linear combination of decoupled effects:

$$\dot{e}_{\text{orb}} = \dot{e}_{\text{gr}} + \dot{e}_{\text{tidal}} + \dot{e}_{\text{eMT}}, \quad (6)$$

where  $\dot{e}_{\text{gr}}$  is from gravitational wave radiation,  $\dot{e}_{\text{tidal}}$  indicates tidal circularization, and  $\dot{e}_{\text{eMT}}$  is due to non-conservative eMT from Equation 4. Models which circularize ( $e = 0$ ) have  $\dot{e}_{\text{eMT}} = 0$  since the equations of Sepinsky et al. 2009 are formally invalid in this regime.

### 2.3. MESA Binary and Stellar Evolution Physics

We use MESA inlists developed for the state-of-the-art Binary Population Synthesis (BPS) code POSYDON version 2 (v2) (Andrews et al. 2024), which implements the results of detailed binary stellar evolution MESA simulations in a framework for large-scale BPS. We leverage the POSYDON software infrastructure to simulate and analyze MESA simulations of H-rich stars with CO companions at solar metallicity  $Z = 0.0142$  (Asplund et al. 2009). According to the adopted MESA simulation setup, the binary is initialized in a tidally locked state with angular momentum loss occurring solely via stellar winds. Once the donor experiences RLO (defined as  $\log_{10}(\dot{M}/M_{\odot} \text{ yr}^{-1}) = -10$ ), we apply all sources of angular momentum transport including spin-orbit coupling, magnetic braking, and gravitational waves, in addition to mass loss. This procedure was designed to match the properties of binaries determined to enter RLO from population synthesis calculations in the POSYDON framework (Fragos et al. 2023; Andrews et al. 2024).

We parameterized the tidal timescale developed from the linear theory (Zahn 1977; Hut 1981; Rasio et al.

1996; Hurley et al. 2002), where the synchronization timescale of the entire model is then taken to be the mass-weighted average of synchronization timescales in each cell, taking the shortest between the dynamical and equilibrium tides. We implement both spin-orbit coupling and (if the donor star has a mass  $< 1.5 M_{\odot}$ ) magnetic braking. For a complete description of all stellar and binary physics, we refer the reader to Fragos et al. 2023; Andrews et al. 2024.

COs are modeled as point masses (i.e., their properties other than mass are ignored) and are allowed to accrete up to their Eddington limit ( $\dot{M}_{\text{Edd}}$ ), above which material is assumed to be lost in an isotropic wind with the specific angular momentum of the accretor. We define the Eddington limit via the relation:  $\eta \dot{M}_{\text{Edd}} c^2 = 4\pi GMc/\kappa$ , where  $\eta$  is the efficiency of converting rest-mass energy to radiation defined as  $\eta = \frac{GM}{Rc^2}$ ,  $c$  is the speed of light,  $M$  and  $R$  define the mass and accretion radius of the central object, and we assume the Roseland mean opacity,  $\kappa$ , is dominated by Thompson scattering  $\kappa = 0.2(1 + X) \text{ cm}^2 \text{ g}^{-1}$ , where  $X$  is the hydrogen abundance of the star. The COs with masses below  $2.5 M_{\odot}$  are assumed to be neutron stars (NSs) with accretion radii of 12 km, while COs above  $2.5 M_{\odot}$  are assumed to be black holes (BHs) with accretion radii set by their innermost stable circular orbit (see 4.2.3; Fragos et al. 2023).

#### 2.3.1. Calculating the Mass Transfer Rate

In the secular orbital evolution equations, we must determine the magnitude of the delta function MT rate at periastron:  $\dot{M}_0$ . We use the eccentric orbit-averaged MT rate adapted from Ritter (1988); Kolb & Ritter (1990) as implemented in the MESA binary module (Paxton et al. 2015). The MT rate is calculated at instantaneous points along the orbit assuming the standard Roche geometry (Eggleton 1983):

$$\mathcal{R}_L = D(v) \frac{0.49q^{2/3}}{0.6q^{2/3} + \ln(1 + q^{1/3})}, \quad (7)$$

where  $D(v) = a(1 - e^2)/(1 + e \cos v)$  is the distance between the mass centers of the two objects as a function of the mean anomaly. Although deviations from this Roche geometry are known to occur in eccentric orbits, Sepinsky et al. 2007a showed they are relatively small on the order of a few percent for a large range of  $q$ . Additionally, other hydrodynamical effects may complicate the picture in determining an accurate MT rate in eccentric orbits (e.g., Lajoie & Sills 2011; Davis et al. 2013; Saladino & Pols 2019), as well as detailed MT stream trajectories (Sepinsky et al. 2010). Due to these uncertainties, we leave more complex treatments of the MT to future work. We discuss this more in Section 5.



#### 2.4. POSYDON Binary Population Synthesis Physics

To obtain astrophysically motivated parameters for binaries hosting COs, we perform an astrophysically motivated BPS simulation with the state-of-the-art POSYDON framework (Fragos et al. 2023; Andrews et al. 2024). Our treatment of BPS physics closely follows that of Rocha et al. 2024, which showed agreement with many observed properties of the Galactic Be X-ray binary population. However, we make one major change to their input physics, using the supernova (SN) remnant prescription of Sukhbold et al. 2016 which allows for the formation of low-mass BHs. Additionally, we assume a burst (instead of constant) star formation history and evolve all binaries to 10 Gyr to sufficiently explore the range of binary configurations which experience eMT. In the following, we reiterate the other key physics assumed in our POSYDON BPS model, and refer a reader to Rocha et al. 2024 for a complete description.

Initial binary component masses and orbital configurations are drawn from observationally motivated distributions: primary masses are drawn from a Kroupa power-law (Kroupa 2001) with  $\alpha = 2.3$  with  $M_1/M_\odot \in [7-120]$ , secondary masses are drawn uniformly  $q \in [0, 1]$  Sana et al. (2013) with a minimum of  $1 M_\odot$ , initial  $P_{\text{orb}}/d \in [1 - 10^{3.5}]$  following a flat-in-log distribution in the range [1-0.35] days following Fragos et al. 2023, and eccentricities are all initially zero with stellar spins synchronized to the orbital period.

Common envelope evolution is modeled with the  $\alpha_{\text{CE}} - \lambda_{\text{CE}}$  formalism (Webbink 1984; Livio & Soker 1988), where we set the fraction of orbital energy used to unbind the envelope  $\alpha_{\text{CE}} = 1$  and the binding energy parameter  $\lambda_{\text{CE}}$  is calculated directly from stellar profiles from our binary MESA simulations in POSYDON.

Supernovae explosions are modeled using the remnant prescription of Sukhbold et al. 2016 for core-collapse SNe (CCSNe), and the remnant prescription of Podsiadlowski et al. 2004 for electron-capture SNe (ECSNe) for He core masses between  $1.4-2.5 M_\odot$ . NSs are given natal kicks resulting from the SN explosion drawn from a Maxwellian with a dispersion of  $\sigma_{\text{CCSNe}} = 265 \text{ km s}^{-1}$  (Hobbs et al. 2005), and a dispersion of  $\sigma_{\text{ECSNe}} = 20 \text{ km s}^{-1}$  (Giacobbo & Mapelli 2019). BHs receive natal kicks with the same dispersion  $\sigma_{\text{CCSNe}}$ , scaled by the BH mass  $M_{\text{BH}}$  with  $1.4 M_\odot/M_{\text{BH}}$ , following Fragos et al. (2023).

##### 2.4.1. Selecting Eccentric Binary Initial Conditions

Since some fraction of binaries hosting COs may naturally circularize from tidal evolution before initiating eMT, we select a subset of binaries from our POSYDON BPS model (Fragos et al. 2023; Andrews et al. 2024).

We take binary parameters ( $M_1$ ,  $M_2$ ,  $P_{\text{orb}}$ , and  $e$ ) at the onset of RLO (oRLO)<sup>1</sup> for systems with  $e > 0.05$  (representing orbits that we consider as “eccentric”) as initial conditions for our eMT MESA simulations to further investigate their evolution. Within POSYDON, oRLO in an eccentric orbit is determined when the star’s radius is 95% of the Roche lobe radius Equation 7. We implicitly account for the evolutionary state of the donor at oRLO in POSYDON (e.g. during post-MS expansion) within the setup of our MESA simulations (see Section 2.3).

In practice, the population of CO and star binaries undergoing eMT will depend strongly on the prior MT physics and SN model used in the BPS. Therefore, the comparison in this work between eMT and the standard modeling choice adopted in BPS (Section 2.5) serves as a concrete analysis of the impact of eMT modeling on CO-hosting binaries.

#### 2.5. Comparison to Instant Circularization

Binaries which initiate MT in eccentric orbits are almost always assumed to efficiently circularize due to strong tides that are expected in tight orbits or with evolved, radially extended stellar components (e.g., Verbunt & Phinney 1995).

Thus, the ad hoc assumption of *instantaneous circularization* has been adopted throughout binary evolution simulations, where the initially eccentric orbit (with semi-major axis  $a$  and eccentricity  $e$ ) is instantly made circular with either: (i) the new orbital separation,  $a_c$ , being set equal to the periape separation of the original orbit  $a_c = a(1 - e)$ , or (ii) applying conservation of orbital angular momentum  $a_c = a(1 - e^2)$ .

To estimate the impact of our self-consistent treatment of eMT, we run a set of MESA simulations in both the original eccentric orbital configuration using Equations 3 and 4, and the instantly circularized approximation (i), using the periape separation  $a_c = a(1 - e)$ . We present these comparisons in Section 4.

### 3. PARAMETER STUDY WITH SIMPLIFIED ECCENTRIC MASS TRANSFER

To isolate the effects of eMT, we first run a suite of MESA simulations with neglecting certain physical effects compared to our default evolutionary models (described in Section 2.3; see also Fragos et al. 2023; Andrews et al. 2024). These simplified eccentric mass transfer (s-eMT) simulations neglect: (1) donor rotation, (2) tidal cou-

<sup>1</sup> We choose a threshold between circular and eccentric binaries of  $e = 0.05$  since this more closely resembles the precision of observational measurements to distinguish such systems (e.g., Fortin et al. 2023).

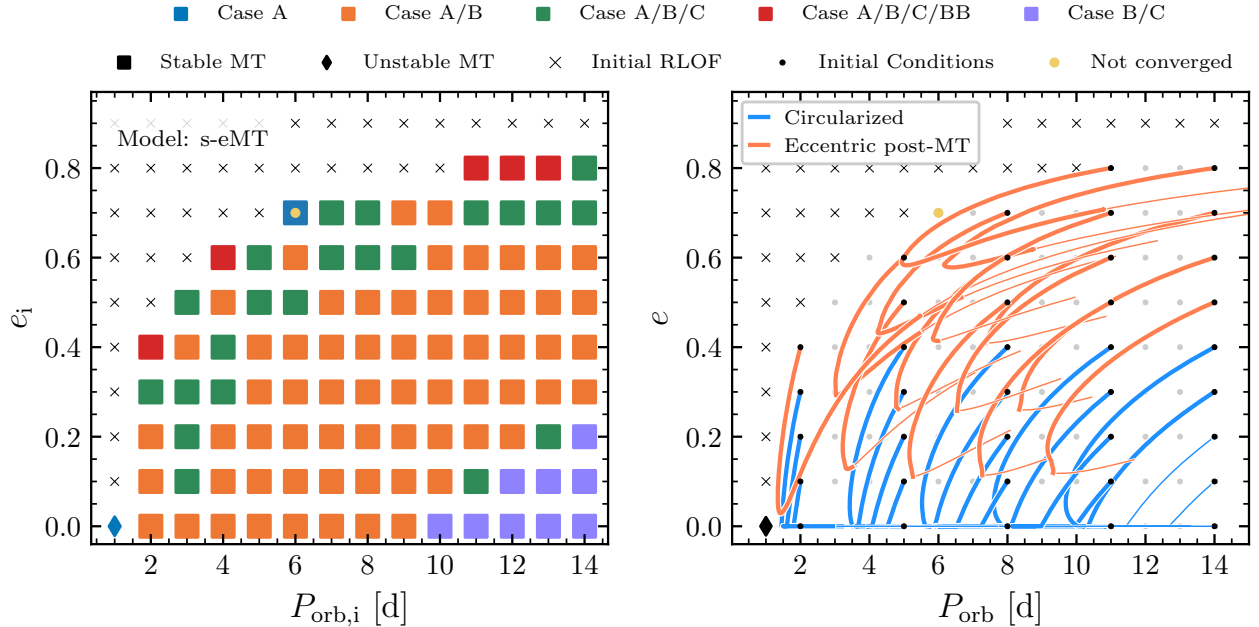


**Figure 1.** Results from our s-eMT binary simulations with  $20 M_{\odot}$  donors and  $10 M_{\odot}$  BHs in various orbital configurations in the  $P_{\text{orb}}-e$  plane, where all orbital evolution is due to the effects of non-conservative eMT (Section 3). The left panel shows the characteristic MT history of our binary simulations (see legend and text), and the right panel shows the time evolution of a subset of models where thick (thin) lines correspond to the MS (post-MS) evolution of a given model (time evolution of gray models are not shown for clarity). After MT, systems with circularized orbits ( $e = 0$ ) are shown in blue, while those with non-zero eccentricities are shown in orange.

pling between the star and orbit, (3) tidal circularization, and (4) wind mass loss from the donor. In practice, this s-eMT setup is close to directly integrating  $\dot{a}_{\text{eMT}}$  and  $\dot{e}_{\text{eMT}}$ , but now the MT rate is calculated self-consistently with a numerical stellar evolution model, unlike the procedure by Sepinsky et al. 2007b, 2009; Hamers & Dosopoulou 2019, where the MT rate was kept constant without numerically solving a stellar structure model.

We consider binaries with a  $10 M_{\odot}$  BH secondary and  $20 M_{\odot}$  MS star primary at orbital periods  $P_{\text{orb}} \in [1-14]$  days and eccentricity  $e \in [0-0.9]$ . Our choice of component masses and orbital periods are motivated by observed high-mass X-ray binaries in the Galaxy (Neumann et al. 2023; Fortin et al. 2023), where the eccentricity is varied to facilitate the present parameter study.

In Figure 1, we show the qualitative results of our simplified models in the  $P_{\text{orb}}-e$  plane, with the MT history of each model indicated by colored symbols (left panel), and the time evolution of a subset of our binary models (right panel). We first consider the MT cases, using the standard definitions: Case A, Case B (Case BB), Case C, where each letter corresponds to oRLO during the MS, before core helium depletion (from a stripped helium star), or in an evolved state post core helium exhaustion, respectively (Iben 1991). Systems that un-

dergo multiple phases of RLO are denoted by multiple letters separated by slashes (e.g. we denote Case A followed by Case B as Case A/B) as introduced in Fragos et al. (2023).

In the left panel of Figure 1, all systems in our simplified model grid go through multiple phases of stable MT (indicated by squares), except for the circular model at  $P_{\text{orb},i} = 1$  day which becomes dynamically unstable (shown by a diamond) while on the MS. Systems which have small initial periastron separations ( $e_i \gtrsim 0.2$  or  $P_{\text{orb},i} \lesssim 10$  days) go through Case A MT, often followed by a second phase of Case B MT initiated by post-MS expansion of the donor, and in systems with the highest eccentricity, Case C into Case BB MT with an evolved helium-rich donor. These MT phases are consistent with other work investigating similar mass ratios in circular configurations (e.g., Qin et al. 2019; Marchant et al. 2021; Gallegos-Garcia et al. 2021), although the orbital evolution is altered due to our accounting for eMT.

In the right panel of Figure 1 we show how binaries with different initial conditions evolve during eMT. We identify two types of evolutionary sequences based off the final orbital configuration of the simulations (prior to the core-collapse of the donor): (1) binaries which circularize due to RLO MT (blue), (2) binaries which remain eccentric post-MT (orange). Systems with ini-

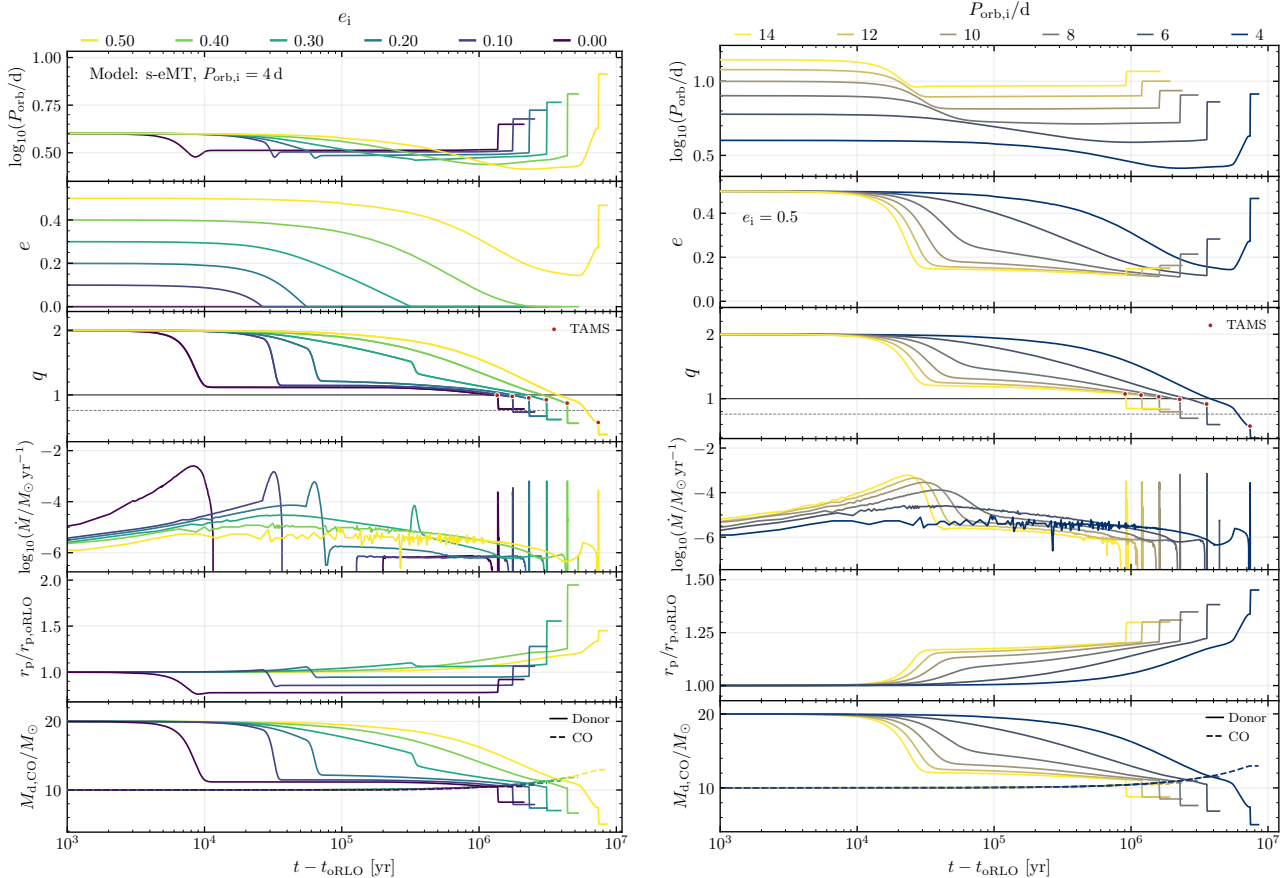


**Figure 2.** Time evolution from oRLO of the orbital period (first row), eccentricity (second row), mass ratio (third row), RLO MT rate (fourth row), the periastron separation normalized by the value at oRLO (fifth row), and the donor and CO masses (last row), for a subset of our s-eMT models with a  $20 M_{\odot}$  donor and  $10 M_{\odot}$  BH shown in Figure 1. The colors in the left column indicate various initial eccentricities and various initial orbital periods in the right column. In the mass ratio ( $q = M_1/M_2$ ) we have indicated with horizontal lines at  $q = 1$  (black) and  $q = 0.76$  (gray dashed) approximate transition points in the sign of  $\dot{a}_{\text{eMT}}$  from Equation 8 and  $\dot{e}_{\text{eMT}}$  from Equation 9. Red points in the  $q$  panels denote when each model reaches TAMS (thick to thin line transitions in Figure 1), which occurs at different times due to the different  $r_{\text{p},i}$  for each model.

tial eccentricities lower (higher) than  $e \simeq 0.35$ , end up circularizing (remain eccentric) by the end of the simulation. We note this circularization is due to the dynamics of eMT, as tides are not included in these simplified runs. In our parameter study this bifurcation between circularized or eccentric orbits post-MT is primarily a function of  $e_i$ , although we expect this behavior may be sensitive to the mass ratio and  $P_{\text{orb},i}$ .

It may also be seen with the time evolution in the  $P_{\text{orb}}-e$  plane that all models follow a similar qualitative behavior: MT initially drives the orbit to shrink (and circularize), but may be followed by a phase of orbital expansion and increasing eccentricity, appearing as a “hook” in the right panel of Figure 1. This behavior can be understood primarily through the evolution of the mass ratio, which has a significant impact on the sign of both  $\dot{a}_{\text{eMT}}$  and  $\dot{e}_{\text{eMT}}$ . In the limit of conservative eMT, Sepinsky et al. 2007b showed the transitional

mass ratio,  $q_{\text{crit}}$ , separating positive and negative rates of change for orbital parameters were found to be well approximated by their Equation (41) for  $\dot{a}_{\text{eMT}}$ :

$$q_{\text{crit}} \simeq 1 - 0.4e + 0.18e^2, \quad (8)$$

and their Equation (42) for  $\dot{e}_{\text{eMT}}$ :

$$q_{\text{crit}} \simeq 0.76 + 0.012e, \quad (9)$$

where any  $q$  above (below) these thresholds will have a positive (negative) rate of change.

To demonstrate this, in Figure 2, we show the time evolution of our s-eMT simulations from oRLO of  $P_{\text{orb}}$ ,  $e$ ,  $q$ , MT rate ( $\dot{M}$ ),  $r_{\text{p}}$  normalized by the periastron separation at oRLO ( $r_{\text{p},\text{oRLO}}$ ), and the component masses ( $M_{\text{d}}$  solid lines,  $M_{\text{CO}}$  dashed lines), for models with varying initial eccentricity (left panel) and initial orbital period (right panel). The line color emphasizes different initial

conditions. The switch from orbital shrinking and circularization to expansion and eccentricity pumping occurs near  $q \simeq 1$  for  $\dot{a}_{\text{eMT}}$  (solid black), and  $q \simeq 0.76$  for  $\dot{e}_{\text{eMT}}$  (gray dashed), both of which are achieved only after significant MT occurs for this binary.

Focusing on systems with varying initial eccentricity and fixed  $P_{\text{orb},i}$  (left column), binaries with higher  $e_i$  (smaller periaapse distances) initiate MT earlier in the donor’s MS lifetime, which corresponds to progressively later times for reaching TAMS (red dots in  $q$ ). This behavior is also reflected in the MT cases in the left panel of Figure 1, where models transition from Case A/B in the most eccentric binaries to Case B/C in the widest orbits (bottom right corner of the  $P_{\text{orb}}-e$  plane). Eccentric orbits also exhibit smaller peak MT rates compared to their circular counterparts due to two effects: (1) the orbit averaged MT rate is lower for more eccentric orbits (with fixed  $r_p$ ; see Equation 7), and (2) the orbital changes in  $P_{\text{orb}}$  and  $e$  result in an increase of the  $r_p$  separation, resulting in an effective widening of the orbit. This second effect is unexpected compared to the classic result, which predicts orbital shrinking for  $q > 1$ . As discussed by Sepinsky et al. 2007b, this can be interpreted physically as a consequence of linear momentum exchange during the MT at periaapse.

This *slower* Case A MT exhibited by more eccentric systems during eMT (low peak  $\dot{M}$  and longer MT timescale) is more conservative than the systems which experience fast Case A MT. This allows the BHs to accrete more mass than predicted in circular systems (dashed lines in the last panels in Figure 2). Binaries with the shortest initial periaapse separations ( $r_{p,i} \lesssim 10 R_{\odot}$ , or binaries which experience Case BB MT in Figure 1) can have BHs accrete up to  $\sim 5 - 9 M_{\odot}$ , nearly doubling their initial mass.

This trend of earlier interaction leading to slower MT is also evident in the right column of Figure 2, where systems with initially short  $P_{\text{orb}}$  experience slow Case A MT, resulting in an anti-correlation between the initial  $P_{\text{orb}}$  and the final eccentricity of the binary. Additionally, since the characteristic evolutionary timescale is governed by MT,  $\tau_{\text{MT}} \propto \dot{M}^{-1}$ , binaries with lower (higher)  $\dot{M}$  evolve slower (faster). This effect can be observed comparing the models with initial  $P_{\text{orb}}$  values of 14 and 4 days, respectively, shown in the right column of Figure 2.

We highlight two key takeaways from this small parameter study: (1) not all binaries will circularize through eMT and may even retain significantly eccentric post-MT, and (2) systems which do not circularize can end their evolution wider and more eccentric than their initial configuration. We see strong correlations between

the initial and final eccentricity and  $P_{\text{orb}}$  of our simplified models, but expect this behavior to be sensitive to the binary component masses, which we do not vary in our s-eMT models.

#### 4. FULL ECCENTRIC MASS TRANSFER BINARY SIMULATIONS

With the characteristic effects of eMT alone established in Section 3, we now run a suite of binary simulations taking into account an expanded set of physical effects, as considered in the POSYDON models: stellar rotation, tidal coupling between the stellar spin and orbital motion, mass and angular momentum loss via stellar winds, as well as angular momentum loss from magnetic braking and gravitational wave radiation.

We consider a population of two hydrogen-rich stars with relatively massive primaries with typical initial conditions (see Section 4.1) which evolves through to the formation of the population’s first COs (NSs or BHs). Following CO formation, most surviving binaries have eccentric orbits due to both mass loss and potential natal kicks imparted to the COs at core collapse. We follow the evolution of systems through their detached phase (details in, Fragos et al. 2023; Andrews et al. 2024) until RLO is initiated at periaapse. At this point we simulate the population in two different ways for comparison: (i) through eMT but this time accounting for the expanded set of physics as aforementioned, and we call these models full eccentric mass transfer (f-eMT) models, and (ii) with the standard BPS ad hoc assumption of instant circularization. This allows us to assess the impact of f-eMT on a realistic, typical population of binaries harboring one compact object and a non-degenerate companion and compare results with the instant circularization assumption that is often made.

For our analysis, we separate f-eMT binaries into two broad outcomes: the population that remains eccentric post-MT in Section 4.2 and those that naturally circularize in Section 4.3. The former outcome is clearly not produced in BPS to date, as systems are forced into circularization. The latter outcome produces circularized systems through eMT; we directly compare these to the circular population from the instant-circularization simulations (Section 2.5).

##### 4.1. Eccentric Binary Population Properties

From our astrophysical POSYDON BPS simulation (Section 2.4), we select models which are instantaneously circularized in POSYDON with a non-degenerate star and CO companion in eccentric orbits during their detached phase post-SN (Section 2.4.1). From our initial binary population of  $4 \times 10^6$  binaries, 16% survive interactions



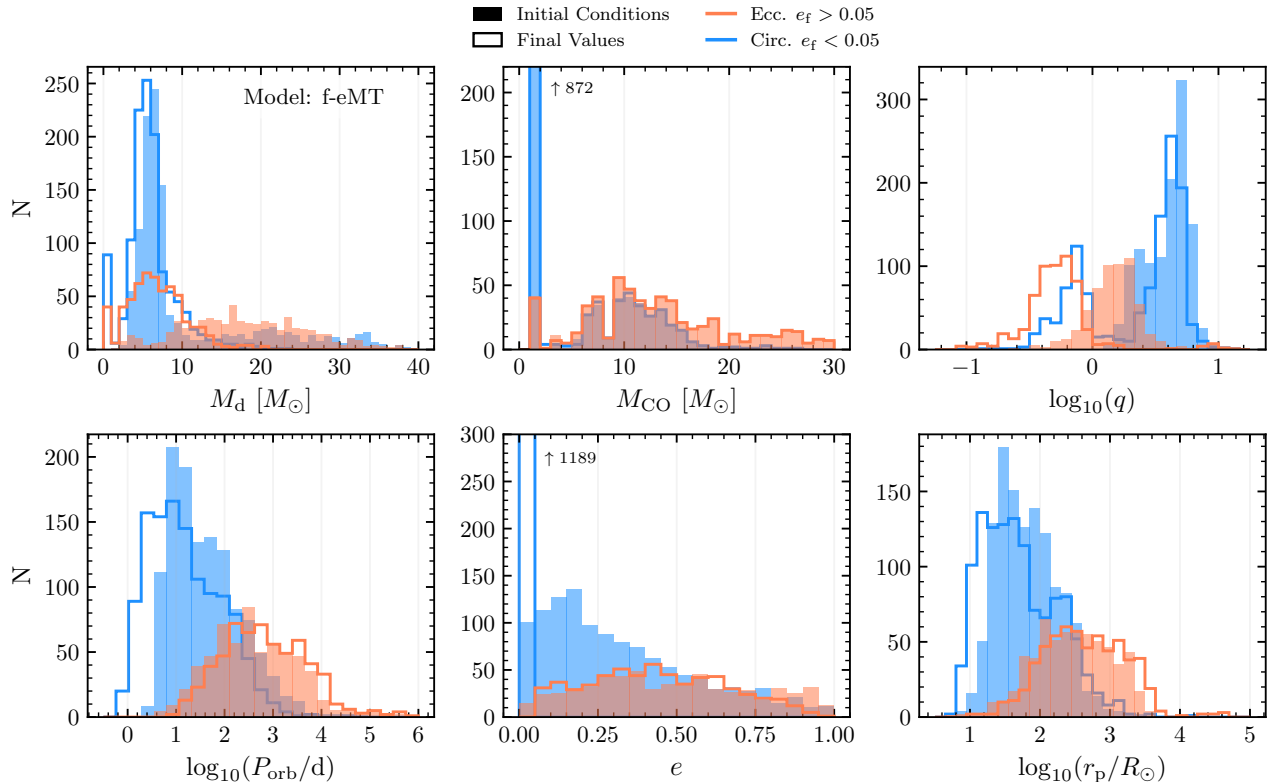


**Figure 3.** One-dimensional distributions of donor star mass (top left), CO mass (top middle), mass ratio between donor and CO mass (top right), orbital period (bottom left), eccentricity (bottom middle), and periape distance (bottom right) for initial binary parameters (filled histograms) and final values (empty histograms) from our binary f-eMT MESA simulations, including secular orbital evolution due to eMT, with self-consistent determination of the MT rate, and additional sources of angular momentum loss (stellar winds, tides, magnetic braking, and gravitational wave radiation; see Section 2.3). Binaries which remain eccentric post-MT are shown in orange and naturally circularized systems in blue, where initial conditions are drawn from an astrophysical POSYDON BPS model (see Section 2.4.1). The end of a binary simulation can be triggered by the donor’s imminent SN, WD formation, or the onset of unstable MT (not shown). The eccentric post-MT binaries constitute 33% of all our astrophysically sampled models.

from the primary’s SN to form binaries containing a CO and a star, hosting either NSs or BHs. Of all the CO-hosting binaries, we find 81% enter RLO at some point in their evolution. About 3/4 (72%) of these RLO systems have residual eccentricity at oRLO ( $e > 0.05$ , Section 2.4.1), which may be considered nominally as eccentric orbits (we take a total of 1791 pair models for direct comparison between f-eMT and instantaneous circularization). Thus, a majority of detached binaries which subsequently undergo MT between a CO and a star in our fiducial BPS model would be subjected to the ad hoc treatment of instantaneous circularization at oRLO, neglecting eMT outcomes.

In Figure A1 we show one-dimensional distributions of the binary population which undergo eccentric RLO from POSYDON (black), and the initial 2000 systems we randomly sample for our MESA models with f-eMT (orange). Our binary models cover a wide range of donor masses ( $M_d/M_\odot \in [1-50]$ ), CO masses with NSs and

BHs ( $M_{CO}/M_\odot \in [1.1-34]$ ), and orbital configurations ( $P_{orb}/d \in [2-10^5]$ ,  $e \in [0.05, 0.99]$ ). The top right panel shows the resulting range of mass ratios with two prominent peaks at  $q \simeq 1-2$  from predominantly BH-hosting binaries, and  $q \simeq 3-8$  with NS-hosting binaries. The most common configuration for a CO and star binary to initiate eMT has a  $P_{orb}$  of 10 days, a modest eccentricity  $e \simeq 0.15$ , with a  $1.2 M_\odot$  NS and  $7 M_\odot$  donor. The overlap of our samples and the underlying astrophysical population show good agreement within the Poisson errors (vertical bars), verifying that our subset of MESA models is representative of the astrophysical BPS.

#### 4.2. Binaries that Remain Eccentric Post-MT

We first focus on binaries which remain eccentric post-MT with  $e_f > 0.05$ , as such systems cannot form under the assumptions of instantaneous circularization. These systems demonstrate that tides and/or eMT itself do not efficiently circularize all binaries. In Figure 3, we

show the initial conditions (filled histogram) and final properties (empty histograms) of this eccentric post-MT population in orange, comprising 33% of the astrophysical population. In all these binaries, the MT remains stable, with most of them (95%) initiating MT during the donor’s post-MS evolution (Case B MT).

This population has low  $q_i$  (upper right panel, orange filled histogram), and is therefore dominated by BH-hosting binaries with high mass donors ( $M_d > 10 M_\odot$ ). Binaries with low mass ratios require less MT to reach the regime where  $\dot{e}_{\text{eMT}}$  changes sign from negative to positive ( $q \simeq 0.76$ , Equation 9), thereby entering a regime where their eccentricity increases rather than reduces, avoiding circularization. Since MT is initiated post-MS, it proceeds rapidly (on a thermal timescale) leading to non-conservative MT (inefficient accretion), explaining the relatively small changes in CO masses (top center panel of Figure 3). This MT history produces stripped, helium-rich donors with two peaks in the final mass distribution:  $M_d \lesssim 1 M_\odot$  forming white dwarfs (WDs), and a wider peak around  $M_d \simeq 6 M_\odot$ , which are massive enough to experience core collapse.

The orbital configurations of the eccentric post-MT population are characterized by wider orbits ( $P_{\text{orb},i}/\text{d} \simeq 10 - 10^4$ , and  $\log_{10}(r_p/R_\odot) > 1.5$ ) with a nearly flat initial eccentricity distribution. At the population level, there is relatively little change between the initial and final orbital parameter distributions, although individual binaries can experience significant evolution in both  $P_{\text{orb}}$  and  $e$  over time.

To demonstrate this, we show in Figure 4 the correlated evolution in the  $P_{\text{orb}}-e$  plane (bottom three panels), selected by their initial mass ratio (corresponding grey bins in the top panel), where orange and blue lines correspond to the eccentric and circularized populations, respectively (as in Figure 3) with starting points of evolution for BH- and NS- hosting binaries marked by circles and pluses, respectively. Similar to the evolutionary sequences identified for our simplified s-eMT models in Section 3, the f-eMT models exhibit phases of both orbital expansion/shrinking and eccentric circularization/pumping primarily understood through the evolution in  $q$ .

We find that binaries with low  $q_i \simeq 1$  (predominantly BH-hosting), remain eccentric throughout their evolution, even post-MT. The reason is that at these mass ratios the values of  $\dot{a}_{\text{eMT}}$  and  $\dot{e}_{\text{eMT}}$  promptly turn positive with very little MT, leading to movement toward the upper right corner of the  $P_{\text{orb}}-e$  plane. This correlated movement causes BH-binaries to end their evolution at larger orbital periods ( $P_{\text{orb}} \simeq 10^2 - 10^4$  days) with more eccentric ( $e \simeq 0.2 - 0.8$ ) orbits. Binaries with

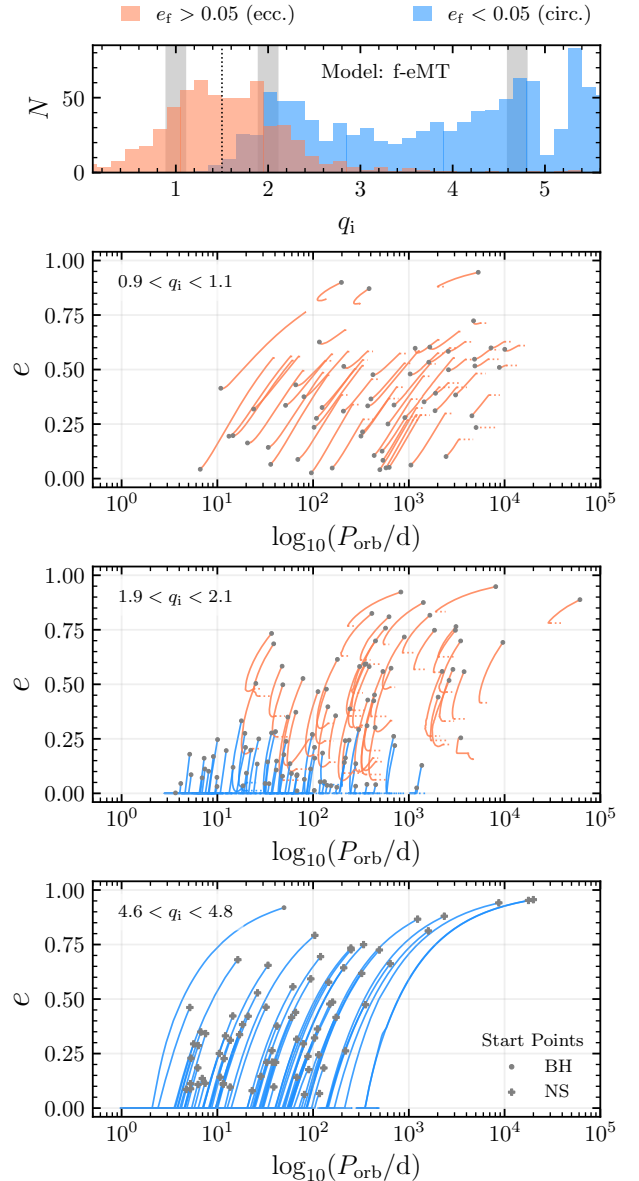


**Figure 4.** Orbital evolution in the  $P_{\text{orb}}-e$  plane for binaries (bottom three panels, for three different initial mass ratio ranges) selected by their initial mass ratio  $q_i$  (top panel), where binaries which circularize or remain eccentric post-MT are shown in blue and orange respectively (as in Figure 3). Solid lines indicate active RLO MT while dotted lines indicate post-MT detached evolution. Systems containing a BH (NS) are marked with a grey dot (plus) at the beginning of the evolution trajectory. The cause of the ‘hook’ evolution is similar to that in our simplified models (see Figure 1, occurring near  $q = 1$ ), but with notable differences due to the inclusion of additional physical effects (e.g., wind mass loss).

larger  $q_i \gtrsim 2 - 3$  (similar to the s-eMT models in Figure 1) initially have negative  $\dot{a}_{\text{eMT}}$  and  $\dot{e}_{\text{eMT}}$ , with only highly eccentric binaries escaping complete circu-

larization. We note that overall, binaries which remain eccentric post-MT but have large  $q_i$  end their evolution in both tighter and wider orbits, but generally experience eccentricity dampening, where the end of MT influences  $e_f$  (see binaries with “hook” evolution in the center  $P_{\text{orb}}-e$  panel of Figure 4).

To understand how models that remain eccentric post-MT ( $e_f > 0.05$ , shown as orange data in Figures 3 and 4) increase or decrease their eccentricity, in Figure 5 we present the distribution of fractional changes in  $e$  from initial to final values through eMT,  $(e_f - e_i)/e_i$ , for binaries hosting BHs (gray) and NSs (purple). The fractional change here is meant to quantify the degree to which a binary system’s eccentricity falls above or below its initial value in our f-eMT models.

Binned by their initial eccentricity, we identify a correlation in BH-hosting systems where low  $e_i$  trends towards greater positive fractional changes (i.e., trends towards  $e_f > e_i$ ). Moving towards greater  $e_i$ , we see this fractional change decreases towards zero and slightly negative at the greatest initial eccentricities ( $e_i \gtrsim 0.8$ ). Thus, systems with greater  $e_i$  show relatively minor changes in their eccentricity through eMT. The variance in the fractional change in  $e$  decreases significantly with increasing  $e_i$ , with 90% of binaries having fractional changes  $\lesssim \pm 25\%$  for  $e_i > 0.8$ . NS-hosting binaries trend toward smaller eccentricities post-MT (i.e.,  $e_f < e_i$ ), which may be seen in the marginal distributions showing the overall trends for BH- and NS-hosting binaries on the right side of Figure 5. This is expected from the larger  $q_i$  of NS-hosting systems, but a few eccentric pumping outcomes (i.e.,  $e_f > e_i$ ) occur at moderate eccentricities for this subpopulation. NS-hosting binaries which remain eccentric post-MT are more prevalent at higher  $e_i \gtrsim 0.6$ , as they can undergo more MT before circularization ( $q$  thresholds from Equation 9).

Motivated by the trends identified in the  $P_{\text{orb}}-e$  plane (Figure 4), we investigate the role of the initial mass ratio,  $q_i$ , on determining outcomes of f-eMT simulations. We show in Figure 6 our eMT models in the  $q_i-e_i$  plane, where we find a clear bifurcation between the eccentric and circularized post-MT populations. We perform a polynomial fit to this bifurcation, characterized as an eccentricity,  $e_{\text{crit}}$ , that is a function of the mass ratio  $q$ :

$$e_{\text{crit}} \simeq -0.210 - 0.729q - 0.1444q^2 - 0.0093q^3 \quad (10)$$

derived from simulations in the range  $q_i \in [0, 5.5]$ . Separating the CO populations, 64% of the BH-hosting binaries remain eccentric post-MT compared to only 5% for NS-hosting binaries.

The bifurcation in  $q_i-e_i$  is evidence that the evolution of our f-eMT models is primarily impacted by the

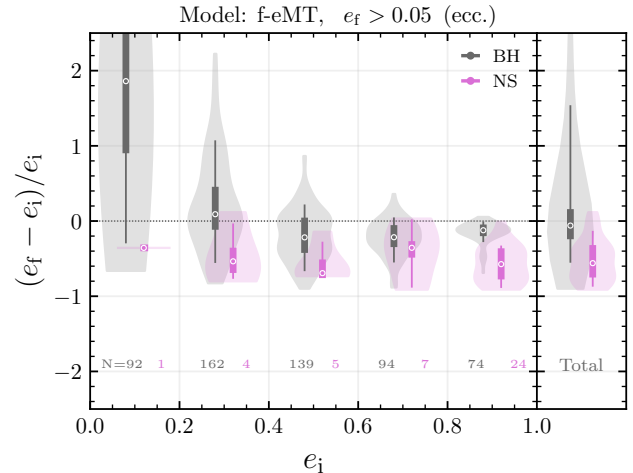


**Figure 5.** For the eccentric post-MT population (orange data in Figure 3): distributions of the fractional change in eccentricity as a function of  $e_i$ , for binaries hosting BHs (gray lines and markers) and NSs (pink lines and markers), with models binned in intervals of  $e_i = 0.2$ , with a small offset in each bin for visual clarity. The full marginal distribution is shown on the right. The median, 68%, and 90% percentiles are shown as circles, thick lines, and thin lines, respectively, while the violin plot shows a kernel density estimate from all points in a bin. Sample counts (N) for BHs and NSs respectively are provided below each violin.

secular orbital evolution from eMT (from Equation 3 and Equation 4) compared to the other sources of angular momentum exchange (stellar winds, tides, magnetic breaking, and gravitational waves). Applying Equation 10 to our s-eMT models (Section 3) with  $q_i = 2$ , the predicted bifurcation eccentricity  $e_{\text{crit}} \simeq 0.4$  agrees reasonably well with the results in Figures 1 and 2. The shape of Equation 10 can be understood to first order, as determined by the competing timescales of changes in eccentricity ( $\tau_e \simeq e/\dot{e}$ ) and mass ratio ( $\tau_{\text{MT}} \simeq M/\dot{M}$ , which can be seen in the prefactor of Equation 4). Binaries with higher  $e_i$  can undergo more MT before complete circularization, reaching low enough  $q$  values to exhibit eccentric pumping (the “hook” evolution in the  $P_{\text{orb}}-e$  plane from Figure 4). Although, analytically deriving this relation is non-trivial due to the inclusion of non-conservative MT and other effects simultaneously evolved within MESA. The few outlier BH models that remain eccentric post-MT but lie in the high  $q_i \simeq 3$  regime (expected to circularize), remain eccentric due to extremely strong stellar winds from high mass donors ( $\gtrsim 20 M_{\odot}$ ), which significantly alter their orbit and mass ratio.

#### 4.3. Binaries that Naturally Circularize

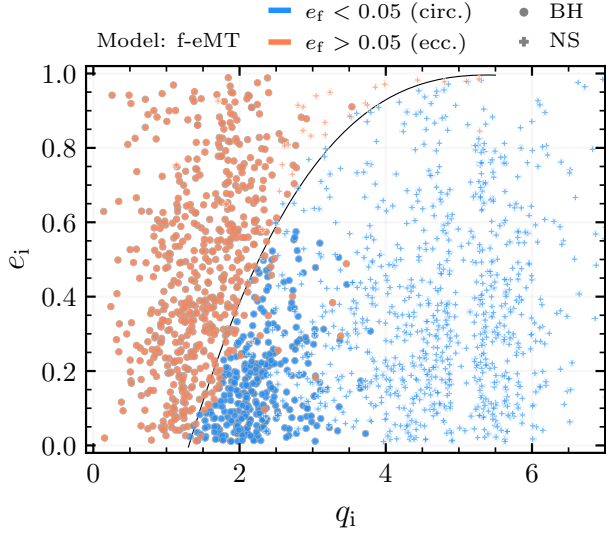


**Figure 6.** Initial conditions for our f-eMT models in initial  $q - e$  plane, color-coded by models that either naturally circularize (blue) or remain eccentric (orange) post-MT as described in Figure 3. Markers indicate binaries hosting BHs (circles) and NSs (pluses). A bifurcation eccentricity,  $e_{\text{crit}}$ , which distinguishes binaries that circularize from those that remain eccentric post-MT, is indicated by the black line. A corresponding fitting function is provided in Equation 10. For BH-hosting binaries, 64% end up remaining eccentric post-MT, while 36% naturally circularize.

We now investigate the subset of binaries that naturally circularize due to eMT (blue distribution in Figure 3), which make up 66% of all our binary simulations sampled with astrophysical initial conditions. These systems are those that can be directly compared to the circular systems produced in the standard BPS population through ad hoc instant-circularization. These naturally circularized binaries from the f-eMT models generally have large initial mass ratios ( $q_i \gtrsim 4$ , which are predominantly NS-hosting binaries), lower  $e_i$  (BH-hosting binaries with small natal kicks), or a combination of both features. This is evident in the  $P_{\text{orb}} - e$  evolution in Figure 4 and in the  $q_i - e_i$  plane from Figure 6. The effects which cause binaries to circularize are described in detail by the evolution in the  $P_{\text{orb}} - e$  plane in Figure 4 and the bifurcation in the  $q_i - e_i$  plane in Figure 6.

First, we consider the MT histories of the models (as in the left panel of Figure 1), which are summarized in Table A1. We find 96% of models agree in their MT history (both evolving through stable or entering dynamically unstable MT) with the remaining 4% having completely divergent evolution. For pair models which agree, we also find that MT cases between models are consistent. In other words, the type of MT (e.g., Case

A, Case B, and Case C) is the same when running the instantly circularized MESA binary model versus f-eMT. Finally, for the pair models which diverge, our f-eMT treatment results in more stable MT ( $\sim 72\%$ ) compared to the instant circularization treatment leading to unstable MT (i.e., common envelope evolution;  $\sim 21\%$ ). This preference for stability is due to the  $r_p$  evolution seen in Figure 2, which effectively widens the binary while residual eccentricity remains in the orbit.

We also consider the differences in final properties of our naturally circularized models and their corresponding models which were instantly circularized (Section 2.5). Our binary MESA simulations are stopped based on variety of criteria related to the formation of a WD, the imminent core collapse of the primary, and the onset of dynamically unstable MT (for details, see Fragos et al. 2023; Andrews et al. 2024). Thus, we compare the final outcomes of a quantity  $\mathbf{x}$  between our f-eMT simulations ( $\mathbf{x}_{\text{eMT}}$ ) and their equivalent instantly circularized MESA models ( $\mathbf{x}_{\text{instant circ}}$ ) by computing the fractional changes between the two cases which we denote with  $\delta$ :

$$\delta \mathbf{x} = \frac{\mathbf{x}_{\text{eMT}} - \mathbf{x}_{\text{instant circ}}}{\mathbf{x}_{\text{instant circ}}}, \quad (11)$$

where we compute the differences relative to the instantly circularized case, as this is the standard assumption in binary stellar evolution. For clarity, we only compute differences between models with matching MT histories (both stable or unstable MT, see Table A1).

In Figure 7, we present one-dimensional histograms for the fractional differences in final donor mass  $\delta M_d$ , orbital period  $\delta P_{\text{orb}}$ , and orbital separation  $\delta a$ , separated by stable or unstable MT. The binaries undergoing stable MT may go on to experience the donor’s core collapse or WD formation, while binaries undergoing unstable MT enter common envelope evolution.

Our naturally circularized f-eMT simulations predict similar donor masses to the instantly circularized case, with 90% of models having  $\delta M_d \lesssim \pm 20\%$ , with medians at about  $\lesssim \pm 5\%$ . The stable MT binaries have smaller  $\delta M_d$  and are positively skewed compared to unstable MT models which have larger absolute  $\delta M_d$  skewing negative. Additionally, f-eMT simulations overwhelmingly predict  $\delta P_{\text{orb}} > 0$ , for both stable and unstable MT distributions, with much larger fractional changes (90% from  $\delta P_{\text{orb}} \simeq 50 - 100\%$  and  $\delta a \simeq 25 - 55\%$ ). Therefore, even binaries which naturally circularize during eMT have different parameters compared to the ad hoc instant circularization approach for both unstable and stable MT systems.

#### 4.3.1. Divergent Evolution



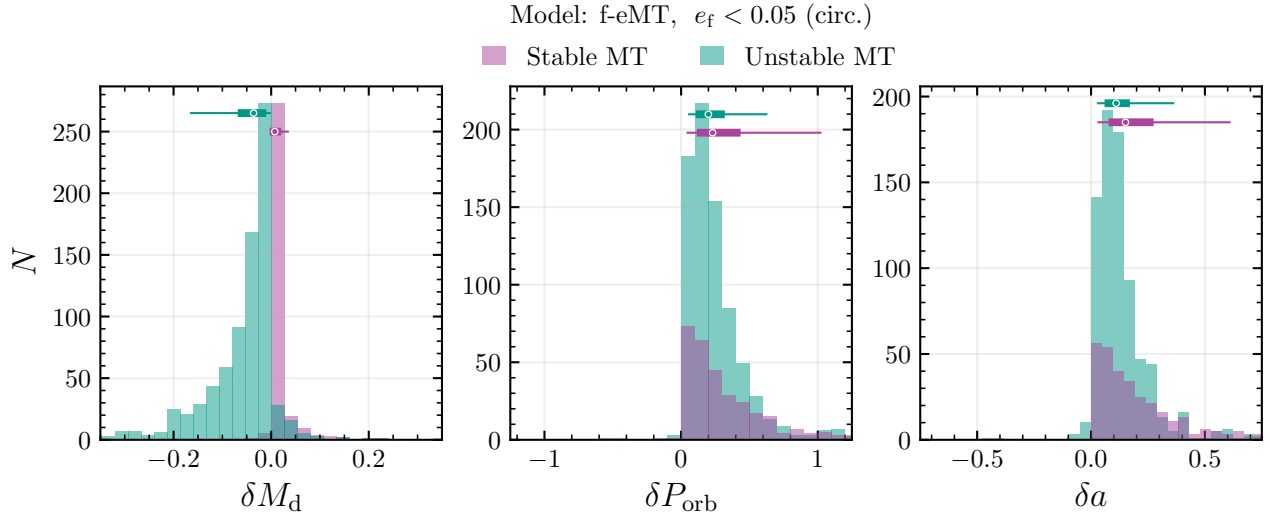


**Figure 7.** For models which naturally circularize in our f-eMT simulations (blue in Figure 3): fractional change (Equation 11) in donor mass (left panel), orbital period (center panel), and semi-major axis (right panel) relative to the instantaneously circularized treatment at the end of each simulations. Positive (negative) values indicate increases (decreases) in a given parameter when using f-eMT compared to instant circularization. Colors indicate simulations where both models undergo stable (purple) or unstable MT (green), where the distribution median, 68%, and 90% percentiles are shown near the top of each histogram (as described in Figure 5).

In Figure 8, we show three example binaries that exhibit completely divergent evolution (i.e. one model has stable MT while the other becomes dynamically unstable) when modeled with f-eMT (colored lines) compared to the equivalent instantly circularized approximation (black). The f-eMT simulations often exhibit lower peak  $\dot{M}$  due to the increase in  $r_p$ , while circular binaries always initially shrink when  $q > 1$ .

The left column of Figure 8 shows a binary with a high mass donor ( $M_d \simeq 13 M_\odot$ ) and a low-mass BH ( $M_{\text{CO}} \simeq 4 M_\odot$ ) with high  $e_i \simeq 0.9$ , undergoing stable Case A/B MT. In this case, the lower peak  $\dot{M}$  in the f-eMT model results in the BH accreting approximately  $0.5 M_\odot$ . The corresponding instantly circularized binary evolves similarly until  $\log_{10}(\dot{M}/M_\odot \text{ yr}^{-1}) \gtrsim -6$ , at which point the shrinking separation drives a runaway increase in the MT rate. The original binary with  $P_{\text{orb},i} \simeq 10^2 \text{ d}$  is significantly impacted by the instant circularization treatment, which arbitrarily reduces the initial orbit to  $P_{\text{orb},\text{circ}} \simeq 3 \text{ d}$ .

The middle column of Figure 8 shows a binary hosting a massive donor  $M_d \simeq 25 M_\odot$ , but with a more massive BH ( $M_{\text{CO}} \simeq 13 M_\odot$ ) and lower  $e_i \simeq 0.2$ . Shortly after Case A MT begins, the f-eMT model naturally circularizes. However, due to the larger orbital period of the f-eMT model (since instant circularization reduces the semi-major axis,  $a_c = a(1 - e)$ ), the post-MS Case B evolution (at  $t - t_{\text{ORLO}} \simeq 3 \times 10^5 \text{ yr}$ ) is stable, whereas the instantly circularized model is deemed to enter dy-

namically unstable MT due to  $L_2$  overflow, which occurs when the donor star radius exceeds the second Lagrangian point.

The final column of Figure 8 shows a binary containing a low-mass donor  $M_d \simeq 3 M_\odot$  and a  $1.3 M_\odot$  NS with moderate eccentricity ( $e_i \simeq 0.5$ ), where the f-eMT simulation eventually becomes unstable during Case B MT, while the instantly circularized model remains stable. The sharp increase in MT near  $\log_{10}(\dot{M}/M_\odot \text{ yr}^{-1}) \gtrsim -5$  occurs when the increase of  $r_p$  (see Section 3) ceases abruptly at  $e = 0$ , where further MT rapidly shrinks the orbit in a runaway process. Before this sharp spike in MT,  $r_p$  decreases due to strong spin-orbit coupling, which spins up the donor. The instantly circularized model artificially escapes a runaway MT episode due to the higher average  $\dot{M}$  throughout the MT phase, reaching a low enough  $q$  to switch from orbital shrinking to expansion.

## 5. DISCUSSION AND CONCLUSIONS

We have implemented the secular orbital evolution equations for non-conservative eMT from Sepinsky et al. 2009, into self-consistent stellar evolution calculations for the first time using MESA. Our focus is on binaries containing COs and non-degenerate donors. Our investigation is divided into two parts: (i) a small parameter study with simplified physics where all orbital evolution is restricted to that induced by non-conservative eMT (Section 3); and (ii) a full-physics grid with astrophysical initial conditions drawn from a POSYDON BPS

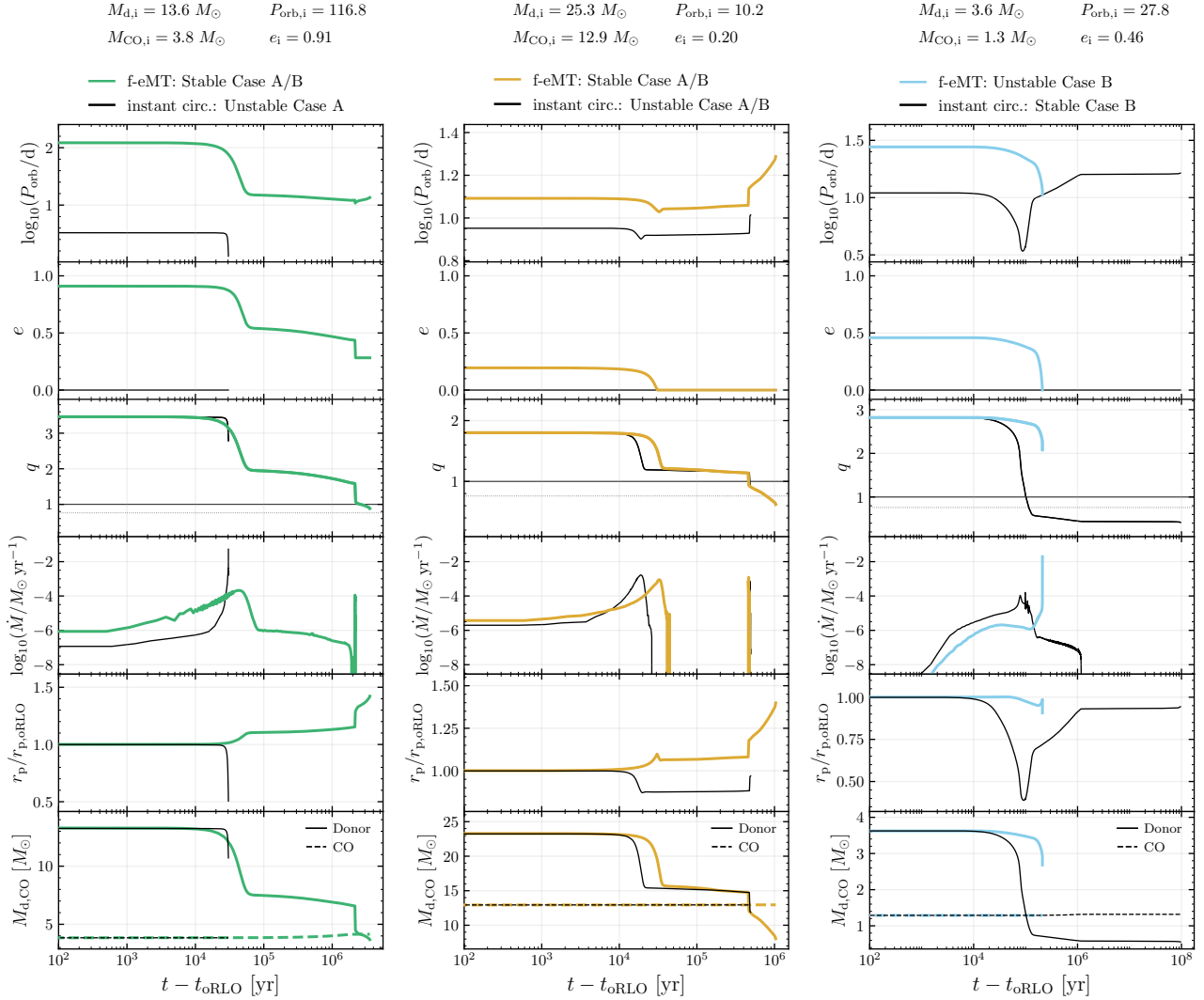


**Figure 8.** Time series evolution of three binaries which have divergent evolution between f-eMT (colored lines) and their equivalent instantly circularized evolution (black) with initial conditions of the original eccentric orbit at the top of each column. Instantly circularized models are adjusted such that  $a_c = a(1 - e)$ . The majority of models which have divergent evolution are biased toward stable MT in the eccentric case (72%), and unstable in the instantly circularized case (21%). In the first binary (left), the trend of increasing  $r_p$  allows the f-eMT model to remain stable. The second (center) binary naturally circularizes  $e = 0$  but the larger  $P_{\text{orb},i}$  compared to the instant circularization allows the eccentric model to survive Case B MT. The last binary (right) becomes unstable once  $e = 0$  due to the lack of increasing  $r_p$  once this limit is hit, while the instantly circularized model transfers enough mass to avoid runaway MT.

of CO-hosting binaries that are found to initiate MT while eccentric (Section 4). The key findings from this modeling are as follows:

1) **s-eMT model:** In the s-eMT simulations containing a  $10 M_\odot$  BH and  $20 M_\odot$  donor, we find novel behavior when including self-consistent modeling of the MT rate from a MESA stellar evolution model in combination with the orbital evolution due to eMT. For binaries with high  $e_i$ , eMT reduces  $q$  before circularizing, allowing  $\dot{a}_{\text{eMT}}$  and  $\dot{e}_{\text{eMT}}$  to become positive. This causes the binaries to remain eccentric post-MT, with some sys-

tems experiencing eccentric pumping, where  $e_f > e_i$ . Remarkably, while binaries are eccentric during MT, the combined changes in  $P_{\text{orb}}$  and  $e$  cause an effective *increase* of  $r_p$ . In contrast, the canonical circular case,  $\dot{a}$  is negative for  $q \gtrsim 1$ . This widening of the orbit tends to stabilize the binary to MT, and in some cases leads to orders-of-magnitude lower MT rates (compared to the circular case; up to a reduction of  $\sim 2.5$  dex in Figure 2), proceeding on the nuclear timescale for systems experiencing Case A MT. For the highly eccentric models, the lower MT rate allows some BHs to accrete more conser-

vatively, nearly doubling their mass before the donor’s core-collapse episode.

2) **f-eMT model:** The majority of evolutionary effects identified in our s-eMT simulations also persist in our f-eMT simulations. The initial conditions of our f-eMT simulations were drawn from an astrophysical BPS model, where  $> 70\%$  of all interacting CO-hosting binaries initiated eMT, suggesting eMT may strongly impact CO binary populations. Most binaries from our astrophysical population initiate post-MS MT (Case B or Case C MT), due to the wider orbital separations of binaries which experience eMT. We find that about one-third of binaries remain eccentric post-MT, while the remaining two-thirds naturally circularize during eMT, with this division depending strongly on the assumed BPS physics. While the eccentric post-MT population categorically diverges from the ad hoc treatment of instantaneous circularization (the ubiquitously adopted approximation), even models which naturally circularize through eMT see notable differences in their final properties (with the 90% distributions around  $\delta M_d \simeq -20\%$  and  $\delta P_{\text{orb}} \simeq 100\%$ ). A smaller fraction of binaries (about 5% of the naturally circularized binaries) exhibit completely divergent evolution (compared to the instantly circularized approach), with eMT generally predicting MT stability over instability in 80% of cases.

3) **A bifurcation in orbital evolution outcomes:** To determine which binaries are likely to remain eccentric post-MT or become naturally circularized, we find these outcomes are strikingly well separated in the  $q_i - e_i$  plane. We have provided a fitting function in Equation 10 so that other studies (e.g. BPS simulations) may estimate the impact of eMT to first-order on different subpopulations such as gravitational wave sources and X-ray binary populations. However, as we have shown, even models which are naturally circularized through eMT can be significantly misrepresented by the ad hoc approach of instant circularization in the predicted donor masses and orbital configurations prior to SN or common-envelope.

4) **Behavior of systems containing a BH:** Approximately 60% of all BH-hosting binaries in the f-eMT models remain eccentric post-MT. Due to their low  $q_i$ , BH-hosting binaries are more likely to remain eccentric post-MT than NS-hosting binaries which predominantly circularize. These BH-hosting binaries are also likely to undergo eccentric pumping and orbital expansion, with  $P_{\text{orb}} \gtrsim 10^2$  days and  $0.2 \lesssim e \lesssim 0.8$ . This type of evolution may be relevant to some of the wide Gaia BH sys-

tems in recent discoveries (El-Badry et al. 2023a,b; Gaia Collaboration et al. 2024), although our models would be relevant to BH companions that have been affected by MT. Future work incorporating eMT into MESA to simulate interactions between two non-degenerate stars will provide more direct comparisons to the wide Gaia binaries hosting COs.

This investigation into the effects of eMT on binary populations indicates that a wide range of CO populations may be impacted by this new treatment. For example, LMXB populations with wide circular orbits, or potential X-ray binary populations with eccentric and moderately wide orbits which may exhibit very low X-ray duty cycles (approximately  $t_{\text{peri}}/P_{\text{orb}}$ ). These binaries primarily initiate post-MS MT, leading to a short-lived X-ray transient stage followed by a detached quiescent phase with stripped helium donors at all eccentricities and wide periods (10 to  $10^4$  days). Given the selection effects that strongly bias against detecting wide binaries and helium stars (Götberg et al. 2018; Drout et al. 2023), it is unsurprising that no such binary has yet been discovered. However, future studies with detailed models for the X-ray emission from binaries undergoing eMT are necessary for drawing more robust conclusions.

In addition to XRBs, eccentric binaries containing BHs have been proposed to explain a special subclass of transient with late time non-thermal emission: fast luminous blue optical transients (e.g., Lazzati et al. 2024). Our results suggest an increased prevalence of these peculiar transients compared to standard binary stellar evolution models as we have shown that BH-binaries are more likely to remain eccentric post-MT.

One key assumption of our model for eMT assumes all MT occurs in a delta function at periape. Although hydrodynamical studies have shown the MT rate in eccentric binaries resembles a Gaussian profile as a function of the true anomaly (e.g. with FWHM  $\sim 0.12 P_{\text{orb}}$  Lajoie & Sills 2011), simulations often cover a single binary configuration and/or resolve too few orbits to determine secular orbital evolution (Lajoie & Sills 2011; Davis et al. 2013; Saladino & Pols 2019). Analytic work extending beyond the assumption of delta function MT are presently unable to account for non-conservative MT (Hamers & Dosopoulou 2019), which is important for binaries hosting COs (Marino et al. 2017; Ziłkowski & Zdziarski 2018, e.g.,). Other secular effects such as those introduced by circumbinary disks from the aforementioned non-conservative accretion (e.g., Valli et al. 2024) or more detailed treatment of tides in eccentric orbits (e.g., MacLeod et al. 2022; Sciarini et al. 2024) may lead to more complex behavior.

While including eMT within the POSYDON framework is our ultimate goal, simply including another dimension into our detailed binary grids is currently too computationally expensive. Nevertheless, exploring more dimensions in binary stellar evolution such as eccentricity is important for our interpretation of modern astrophysical populations (e.g., de Sá et al. 2024). Machine learning algorithms like active learning may be necessary to facilitate expansions to higher dimensions within the POSYDON framework (Rocha et al. 2022).

Combining all results from our f-eMT simulations, we conclude eMT is important to consider for the evolutionary history of CO-hosting binaries (e.g. low-mass/high-mass X-ray binaries, binary black hole mergers, gamma-ray burst progenitors) which are thought to have at least one phase of RLO MT. In future work we will implement the eMT formalism into MESA to simulate interactions between two non-degenerate stars. In this regime, we plan to investigate the large population of wide post-interaction binaries observed to contain stripped donors and WDs.

#### ACKNOWLEDGMENTS

KAR, SG, and MS are supported by the Gordon and Betty Moore Foundation (PI Kalogera, grant awards GBMF8477 and GBMF12341) and CIERA’s Riedel Family Fellowship in Data Science. DM and KAR thank the LSSTC Data Science Fellowship Program, which is funded by LSSTC, NSF Cybertraining Grant No. 1829740, the Brinson Foundation, and the Moore Foundation; their participation in the program has benefited this work. KAR is also supported by the NASA grant awarded to the Illinois/NASA Space Grant Consortium, and any opinions, findings, conclusions, or recommendations expressed in this material are those of the author and do not necessarily reflect the views of NASA. JJA acknowledges support for Program num-

ber (JWST-AR-04369.001-A) provided through a grant from the STScI under NASA contract NAS5-03127. VK was partially supported through the D.I.Linzer Distinguished University Professorship fund. S.B., M.B., T.F., M.K., and Z.X. acknowledge support by the Swiss National Science Foundation (PI Fragos, project number CRSII5\_213497). KK and EZ were partially supported by the Federal Commission for Scholarships for Foreign Students for the Swiss Government Excellence Scholarship (ESKAS No. 2021.0277 and ESKAS No. 2019.0091, respectively). KK is supported by a fellowship program at the Institute of Space Sciences (ICE-CSIC) funded by the program Unidad de Excelencia María de Maeztu CEX2020-001058-M. Z.X. was supported by the Chinese Scholarship Council (CSC). Support for M.Z. was provided by NASA through the NASA Hubble Fellowship grant HST-HF2-51474.001-A awarded by the Space Telescope Science Institute, which is operated by the Association of Universities for Research in Astronomy, Incorporated, under NASA contract NAS5-26555.

The computations were performed at Northwestern University on the Trident computer cluster (funded by the GBMF8477 award). This research was supported in part through the computational resources and staff contributions provided for the Quest high performance computing facility at Northwestern University which is jointly supported by the Office of the Provost, the Office for Research, and Northwestern University Information Technology. We thank Monica Gallegos-Garcia for assisting in the BPS setup for this work and Chase Kimball for helpful comments on the manuscript.

*Software:* NumPy (van der Walt et al. 2011), SciPy (Virtanen et al. 2020), Astropy (Astropy Collaboration et al. 2013, 2018, 2022), matplotlib (Hunter 2007), pandas (pandas development team 2020), POSYDON (Fragos et al. 2023; Andrews et al. 2024), MESA (Paxton et al. 2011, 2015, 2013, 2018, 2019)

#### REFERENCES

- Abbott, R., Abbott, T. D., Acernese, F., et al. 2023, *Physical Review X*, 13, 011048, doi: [10.1103/PhysRevX.13.011048](https://doi.org/10.1103/PhysRevX.13.011048)
- Andrews, J. J., Taggart, K., & Foley, R. 2022, arXiv e-prints, arXiv:2207.00680, doi: [10.48550/arXiv.2207.00680](https://doi.org/10.48550/arXiv.2207.00680)
- Andrews, J. J., Bavera, S. S., Briel, M., et al. 2024, arXiv e-prints, arXiv:2411.02376, doi: [10.48550/arXiv.2411.02376](https://doi.org/10.48550/arXiv.2411.02376)
- Asplund, M., Grevesse, N., Sauval, A. J., & Scott, P. 2009, *ARA&A*, 47, 481, doi: [10.1146/annurev.astro.46.060407.145222](https://doi.org/10.1146/annurev.astro.46.060407.145222)
- Astropy Collaboration, Robitaille, T. P., Tollerud, E. J., et al. 2013, *A&A*, 558, A33, doi: [10.1051/0004-6361/201322068](https://doi.org/10.1051/0004-6361/201322068)
- Astropy Collaboration, Price-Whelan, A. M., Sipőcz, B. M., et al. 2018, *AJ*, 156, 123, doi: [10.3847/1538-3881/aabc4f](https://doi.org/10.3847/1538-3881/aabc4f)
- Astropy Collaboration, Price-Whelan, A. M., Lim, P. L., et al. 2022, *ApJ*, 935, 167, doi: [10.3847/1538-4357/ac7c74](https://doi.org/10.3847/1538-4357/ac7c74)



- Bahramian, A., & Degenaar, N. 2023, in Handbook of X-ray and Gamma-ray Astrophysics, 120, doi: [10.1007/978-981-16-4544-0\\_94-1](https://doi.org/10.1007/978-981-16-4544-0_94-1)
- Bailyn, C. D. 1995, ARA&A, 33, 133, doi: [10.1146/annurev.aa.33.090195.001025](https://doi.org/10.1146/annurev.aa.33.090195.001025)
- Bashi, D., Mazeh, T., & Faigler, S. 2023, MNRAS, 522, 1184, doi: [10.1093/mnras/stad999](https://doi.org/10.1093/mnras/stad999)
- Breivik, K., Coughlin, S., Zevin, M., et al. 2020, ApJ, 898, 71, doi: [10.3847/1538-4357/ab9d85](https://doi.org/10.3847/1538-4357/ab9d85)
- Davis, P. J., Siess, L., & Deschamps, R. 2013, A&A, 556, A4, doi: [10.1051/0004-6361/201220391](https://doi.org/10.1051/0004-6361/201220391)
- de Sá, L. M., Bernardo, A., Rocha, L. S., Bachega, R. R. A., & Horvath, J. E. 2024, MNRAS, doi: [10.1093/mnras/stae2388](https://doi.org/10.1093/mnras/stae2388)
- D’Orazio, D. J., & Duffell, P. C. 2021, ApJL, 914, L21, doi: [10.3847/2041-8213/ac0621](https://doi.org/10.3847/2041-8213/ac0621)
- Dosopoulou, F., & Kalogera, V. 2016, ApJ, 825, 70, doi: [10.3847/0004-637X/825/1/70](https://doi.org/10.3847/0004-637X/825/1/70)
- Drout, M. R., Götberg, Y., Ludwig, B. A., et al. 2023, Science, 382, 1287, doi: [10.1126/science.ade4970](https://doi.org/10.1126/science.ade4970)
- Eggleton, P. P. 1983, ApJ, 268, 368, doi: [10.1086/160960](https://doi.org/10.1086/160960)
- El-Badry, K., Conroy, C., Quataert, E., et al. 2022, MNRAS, 516, 3602, doi: [10.1093/mnras/stac2422](https://doi.org/10.1093/mnras/stac2422)
- El-Badry, K., Rix, H.-W., Quataert, E., et al. 2023a, MNRAS, 518, 1057, doi: [10.1093/mnras/stac3140](https://doi.org/10.1093/mnras/stac3140)
- El-Badry, K., Rix, H.-W., Cendes, Y., et al. 2023b, MNRAS, 521, 4323, doi: [10.1093/mnras/stad799](https://doi.org/10.1093/mnras/stad799)
- Eldridge, J. J., Stanway, E. R., Xiao, L., et al. 2017, PASA, 34, e058, doi: [10.1017/pasa.2017.51](https://doi.org/10.1017/pasa.2017.51)
- Escorza, A., & De Rosa, R. J. 2023, A&A, 671, A97, doi: [10.1051/0004-6361/202244782](https://doi.org/10.1051/0004-6361/202244782)
- Fornasini, F. M., Antoniou, V., & Dubus, G. 2023, arXiv e-prints, arXiv:2308.02645, doi: [10.48550/arXiv.2308.02645](https://doi.org/10.48550/arXiv.2308.02645)
- Fortin, F., García, F., Simaz Bunzel, A., & Chaty, S. 2023, A&A, 671, A149, doi: [10.1051/0004-6361/202245236](https://doi.org/10.1051/0004-6361/202245236)
- Fragos, T., Andrews, J. J., Bavera, S. S., et al. 2023, ApJS, 264, 45, doi: [10.3847/1538-4365/ac90c1](https://doi.org/10.3847/1538-4365/ac90c1)
- Gaia Collaboration, Panuzzo, P., Mazeh, T., et al. 2024, A&A, 686, L2, doi: [10.1051/0004-6361/202449763](https://doi.org/10.1051/0004-6361/202449763)
- Gallegos-Garcia, M., Berry, C. P. L., Marchant, P., & Kalogera, V. 2021, ApJ, 922, 110, doi: [10.3847/1538-4357/ac2610](https://doi.org/10.3847/1538-4357/ac2610)
- Geller, A. M., Leigh, N. W. C., Giersz, M., Kremer, K., & Rasio, F. A. 2019, ApJ, 872, 165, doi: [10.3847/1538-4357/ab0214](https://doi.org/10.3847/1538-4357/ab0214)
- Geller, A. M., Mathieu, R. D., Harris, H. C., & McClure, R. D. 2009, AJ, 137, 3743, doi: [10.1088/0004-6256/137/4/3743](https://doi.org/10.1088/0004-6256/137/4/3743)
- Geller, A. M., Mathieu, R. D., Latham, D. W., et al. 2021, AJ, 161, 190, doi: [10.3847/1538-3881/abdd23](https://doi.org/10.3847/1538-3881/abdd23)
- Giacobbo, N., & Mapelli, M. 2019, MNRAS, 482, 2234, doi: [10.1093/mnras/sty2848](https://doi.org/10.1093/mnras/sty2848)
- Giacobbo, N., Mapelli, M., & Spera, M. 2018, MNRAS, 474, 2959, doi: [10.1093/mnras/stx2933](https://doi.org/10.1093/mnras/stx2933)
- Gosnell, N. M., Mathieu, R. D., Geller, A. M., et al. 2015, ApJ, 814, 163, doi: [10.1088/0004-637X/814/2/163](https://doi.org/10.1088/0004-637X/814/2/163)
- Götberg, Y., de Mink, S. E., Groh, J. H., et al. 2018, A&A, 615, A78, doi: [10.1051/0004-6361/201732274](https://doi.org/10.1051/0004-6361/201732274)
- Hamers, A. S., & Dosopoulou, F. 2019, ApJ, 872, 119, doi: [10.3847/1538-4357/ab001d](https://doi.org/10.3847/1538-4357/ab001d)
- Heber, U. 2009, ARA&A, 47, 211, doi: [10.1146/annurev-astro-082708-101836](https://doi.org/10.1146/annurev-astro-082708-101836)
- Hobbs, G., Lorimer, D. R., Lyne, A. G., & Kramer, M. 2005, MNRAS, 360, 974, doi: [10.1111/j.1365-2966.2005.09087.x](https://doi.org/10.1111/j.1365-2966.2005.09087.x)
- Hu, Z., Zhu, W., Dai, F., et al. 2024, arXiv e-prints, arXiv:2409.18296, doi: [10.48550/arXiv.2409.18296](https://doi.org/10.48550/arXiv.2409.18296)
- Hunter, J. D. 2007, Computing in Science Engineering, 9, 90, doi: [10.1109/MCSE.2007.55](https://doi.org/10.1109/MCSE.2007.55)
- Hurley, J. R., Tout, C. A., & Pols, O. R. 2002, MNRAS, 329, 897, doi: [10.1046/j.1365-8711.2002.05038.x](https://doi.org/10.1046/j.1365-8711.2002.05038.x)
- Hut, P. 1981, A&A, 99, 126
- Hwang, H.-C., Ting, Y.-S., & Zakamska, N. L. 2022, MNRAS, 512, 3383, doi: [10.1093/mnras/stac675](https://doi.org/10.1093/mnras/stac675)
- Iben, Icko, J. 1991, ApJS, 76, 55, doi: [10.1086/191565](https://doi.org/10.1086/191565)
- Ivanova, N., Belczynski, K., Fregeau, J. M., & Rasio, F. A. 2005, MNRAS, 358, 572, doi: [10.1111/j.1365-2966.2005.08804.x](https://doi.org/10.1111/j.1365-2966.2005.08804.x)
- Kolb, U., & Ritter, H. 1990, A&A, 236, 385
- Kretschmar, P., Fürst, F., Sidoli, L., et al. 2019, NewAR, 86, 101546, doi: [10.1016/j.newar.2020.101546](https://doi.org/10.1016/j.newar.2020.101546)
- Kroupa, P. 2001, MNRAS, 322, 231, doi: [10.1046/j.1365-8711.2001.04022.x](https://doi.org/10.1046/j.1365-8711.2001.04022.x)
- Kuiper, G. P. 1941, ApJ, 93, 133, doi: [10.1086/144252](https://doi.org/10.1086/144252)
- Lai, D., & Muñoz, D. J. 2023, ARA&A, 61, 517, doi: [10.1146/annurev-astro-052622-022933](https://doi.org/10.1146/annurev-astro-052622-022933)
- Lajoie, C.-P., & Sills, A. 2011, ApJ, 726, 67, doi: [10.1088/0004-637X/726/2/67](https://doi.org/10.1088/0004-637X/726/2/67)
- Lamberts, A., Blunt, S., Littenberg, T. B., et al. 2019, MNRAS, 490, 5888, doi: [10.1093/mnras/stz2834](https://doi.org/10.1093/mnras/stz2834)
- Langer, N. 2012, ARA&A, 50, 107, doi: [10.1146/annurev-astro-081811-125534](https://doi.org/10.1146/annurev-astro-081811-125534)
- Lazzati, D., Perna, R., Ryu, T., & Breivik, K. 2024, ApJL, 972, L17, doi: [10.3847/2041-8213/ad70ba](https://doi.org/10.3847/2041-8213/ad70ba)
- Linck, E., Mathieu, R. D., & Latham, D. W. 2024, AJ, 168, 205, doi: [10.3847/1538-3881/ad6b1a](https://doi.org/10.3847/1538-3881/ad6b1a)
- Livio, M., & Soker, N. 1988, ApJ, 329, 764, doi: [10.1086/166419](https://doi.org/10.1086/166419)

- Lubow, S. H. 2022, *MNRAS*, 516, 5446, doi: [10.1093/mnras/stac2636](https://doi.org/10.1093/mnras/stac2636)
- Lubow, S. H., & Shu, F. H. 1975, *ApJ*, 198, 383, doi: [10.1086/153614](https://doi.org/10.1086/153614)
- MacLeod, M., Vick, M., & Loeb, A. 2022, *ApJ*, 937, 37, doi: [10.3847/1538-4357/ac8aff](https://doi.org/10.3847/1538-4357/ac8aff)
- Marchant, P., & Bodensteiner, J. 2024, *Annual Review of Astronomy and Astrophysics*, doi: <https://doi.org/10.1146/annurev-astro-052722-105936>
- Marchant, P., Pappas, K. M. W., Gallegos-Garcia, M., et al. 2021, *A&A*, 650, A107, doi: [10.1051/0004-6361/202039992](https://doi.org/10.1051/0004-6361/202039992)
- Marino, A., Di Salvo, T., Gambino, A. F., et al. 2017, *A&A*, 603, A137, doi: [10.1051/0004-6361/201730464](https://doi.org/10.1051/0004-6361/201730464)
- Mathieu, R. D. 1994, *ARA&A*, 32, 465, doi: [10.1146/annurev.aa.32.090194.002341](https://doi.org/10.1146/annurev.aa.32.090194.002341)
- Milliman, K. E., Leiner, E., Mathieu, R. D., Tofflemire, B. M., & Platais, I. 2016, *AJ*, 151, 152, doi: [10.3847/0004-6256/151/6/152](https://doi.org/10.3847/0004-6256/151/6/152)
- Milliman, K. E., Mathieu, R. D., Geller, A. M., et al. 2014, *AJ*, 148, 38, doi: [10.1088/0004-6256/148/2/38](https://doi.org/10.1088/0004-6256/148/2/38)
- Moriya, T. J., Liu, Z.-W., Mackey, J., Chen, T.-W., & Langer, N. 2015, *A&A*, 584, L5, doi: [10.1051/0004-6361/201527515](https://doi.org/10.1051/0004-6361/201527515)
- Muñoz, D. J., & Lithwick, Y. 2020, *ApJ*, 905, 106, doi: [10.3847/1538-4357/abc74c](https://doi.org/10.3847/1538-4357/abc74c)
- Naoz, S., Fragos, T., Geller, A., Stephan, A. P., & Rasio, F. A. 2016, *ApJL*, 822, L24, doi: [10.3847/2041-8205/822/2/L24](https://doi.org/10.3847/2041-8205/822/2/L24)
- Neumann, M., Avakyan, A., Doroshenko, V., & Santangelo, A. 2023, *A&A*, 677, A134, doi: [10.1051/0004-6361/202245728](https://doi.org/10.1051/0004-6361/202245728)
- Nie, J. D., Wood, P. R., & Nicholls, C. P. 2017, *ApJ*, 835, 209, doi: [10.3847/1538-4357/835/2/209](https://doi.org/10.3847/1538-4357/835/2/209)
- Nine, A. C., Mathieu, R. D., Schuler, S. C., & Milliman, K. E. 2024, *ApJ*, 970, 187, doi: [10.3847/1538-4357/ad534b](https://doi.org/10.3847/1538-4357/ad534b)
- Oomen, G.-M., Van Winckel, H., Pols, O., et al. 2018, *A&A*, 620, A85, doi: [10.1051/0004-6361/201833816](https://doi.org/10.1051/0004-6361/201833816)
- Paczyński, B. 1971, *ARA&A*, 9, 183, doi: [10.1146/annurev.aa.09.090171.001151](https://doi.org/10.1146/annurev.aa.09.090171.001151)
- pandas development team, T. 2020, *pandas-dev/pandas: Pandas, latest*, Zenodo, doi: [10.5281/zenodo.3509134](https://doi.org/10.5281/zenodo.3509134)
- Paxton, B., Bildsten, L., Dotter, A., et al. 2011, *ApJS*, 192, 3, doi: [10.1088/0067-0049/192/1/3](https://doi.org/10.1088/0067-0049/192/1/3)
- Paxton, B., Cantiello, M., Arras, P., et al. 2013, *ApJS*, 208, 4, doi: [10.1088/0067-0049/208/1/4](https://doi.org/10.1088/0067-0049/208/1/4)
- Paxton, B., Marchant, P., Schwab, J., et al. 2015, *ApJS*, 220, 15, doi: [10.1088/0067-0049/220/1/15](https://doi.org/10.1088/0067-0049/220/1/15)
- Paxton, B., Schwab, J., Bauer, E. B., et al. 2018, *ApJS*, 234, 34, doi: [10.3847/1538-4365/aaa5a8](https://doi.org/10.3847/1538-4365/aaa5a8)
- Paxton, B., Smolec, R., Schwab, J., et al. 2019, *ApJS*, 243, 10, doi: [10.3847/1538-4365/ab2241](https://doi.org/10.3847/1538-4365/ab2241)
- Podsiadlowski, P., Langer, N., Poelarends, A. J. T., et al. 2004, *ApJ*, 612, 1044, doi: [10.1086/421713](https://doi.org/10.1086/421713)
- Qin, Y., Marchant, P., Fragos, T., Meynet, G., & Kalogera, V. 2019, *ApJL*, 870, L18, doi: [10.3847/2041-8213/aaf97b](https://doi.org/10.3847/2041-8213/aaf97b)
- Raguzova, N. V., & Popov, S. B. 2005, *Astronomical and Astrophysical Transactions*, 24, 151, doi: [10.1080/10556790500497311](https://doi.org/10.1080/10556790500497311)
- Rasio, F. A., Tout, C. A., Lubow, S. H., & Livio, M. 1996, *ApJ*, 470, 1187, doi: [10.1086/177941](https://doi.org/10.1086/177941)
- Ritter, H. 1988, *A&A*, 202, 93
- Rocha, K. A., Andrews, J. J., Berry, C. P. L., et al. 2022, *ApJ*, 938, 64, doi: [10.3847/1538-4357/ac8b05](https://doi.org/10.3847/1538-4357/ac8b05)
- Rocha, K. A., Kalogera, V., Doctor, Z., et al. 2024, *ApJ*, 971, 133, doi: [10.3847/1538-4357/ad5955](https://doi.org/10.3847/1538-4357/ad5955)
- Rodriguez, C. L., Weatherford, N. C., Coughlin, S. C., et al. 2022, *ApJS*, 258, 22, doi: [10.3847/1538-4365/ac2edf](https://doi.org/10.3847/1538-4365/ac2edf)
- Saladino, M. I., & Pols, O. R. 2019, *A&A*, 629, A103, doi: [10.1051/0004-6361/201935625](https://doi.org/10.1051/0004-6361/201935625)
- Sana, H., de Koter, A., de Mink, S. E., et al. 2013, *A&A*, 550, A107, doi: [10.1051/0004-6361/201219621](https://doi.org/10.1051/0004-6361/201219621)
- Sciarini, L., Ekström, S., Eggenberger, P., et al. 2024, *A&A*, 681, L1, doi: [10.1051/0004-6361/202348424](https://doi.org/10.1051/0004-6361/202348424)
- Sepinsky, J. F., Willems, B., & Kalogera, V. 2007a, *ApJ*, 660, 1624, doi: [10.1086/513736](https://doi.org/10.1086/513736)
- Sepinsky, J. F., Willems, B., Kalogera, V., & Rasio, F. A. 2007b, *ApJ*, 667, 1170, doi: [10.1086/520911](https://doi.org/10.1086/520911)
- . 2009, *ApJ*, 702, 1387, doi: [10.1088/0004-637X/702/2/1387](https://doi.org/10.1088/0004-637X/702/2/1387)
- . 2010, *ApJ*, 724, 546, doi: [10.1088/0004-637X/724/1/546](https://doi.org/10.1088/0004-637X/724/1/546)
- Simaz Bunzel, A., García, F., Combi, J. A., & Chaty, S. 2023, *A&A*, 670, A80, doi: [10.1051/0004-6361/202245081](https://doi.org/10.1051/0004-6361/202245081)
- Siwek, M., Weinberger, R., & Hernquist, L. 2023, *MNRAS*, 522, 2707, doi: [10.1093/mnras/stad1131](https://doi.org/10.1093/mnras/stad1131)
- Sukhbold, T., Ertl, T., Woosley, S. E., Brown, J. M., & Janka, H. T. 2016, *ApJ*, 821, 38, doi: [10.3847/0004-637X/821/1/38](https://doi.org/10.3847/0004-637X/821/1/38)
- Sun, M., & Arras, P. 2018, *ApJ*, 858, 14, doi: [10.3847/1538-4357/aab9a4](https://doi.org/10.3847/1538-4357/aab9a4)
- Sun, M., Levina, S., Gossage, S., et al. 2024, *ApJ*, 969, 8, doi: [10.3847/1538-4357/ad47c1](https://doi.org/10.3847/1538-4357/ad47c1)
- Sun, M., & Mathieu, R. D. 2023, *ApJ*, 944, 89, doi: [10.3847/1538-4357/acacf7](https://doi.org/10.3847/1538-4357/acacf7)
- Sun, M., Mathieu, R. D., Leiner, E. M., & Townsend, R. H. D. 2021, *ApJ*, 908, 7, doi: [10.3847/1538-4357/abd402](https://doi.org/10.3847/1538-4357/abd402)

- Tang, P., Meyer, R., & Eldridge, J. 2024, arXiv e-prints, arXiv:2411.02563, doi: [10.48550/arXiv.2411.02563](https://doi.org/10.48550/arXiv.2411.02563)
- Tauris, T. M., & van den Heuvel, E. P. J. 2023, Physics of Binary Star Evolution. From Stars to X-ray Binaries and Gravitational Wave Sources, doi: [10.48550/arXiv.2305.09388](https://doi.org/10.48550/arXiv.2305.09388)
- Townsend, R. 2020, MESA SDK for Linux, 20.3.1, Zenodo, doi: [10.5281/zenodo.3706650](https://doi.org/10.5281/zenodo.3706650)
- Valli, R., Tiede, C., Vigna-Gómez, A., et al. 2024, A&A, 688, A128, doi: [10.1051/0004-6361/202449421](https://doi.org/10.1051/0004-6361/202449421)
- van den Heuvel, E. P. J. 2019, in IAU Symposium, Vol. 346, High-mass X-ray Binaries: Illuminating the Passage from Massive Binaries to Merging Compact Objects, ed. L. M. Oskinova, E. Bozzo, T. Bulik, & D. R. Gies, 1–13, doi: [10.1017/S1743921319001315](https://doi.org/10.1017/S1743921319001315)
- Van der Swaelmen, M., Boffin, H. M. J., Jorissen, A., & Van Eck, S. 2017, A&A, 597, A68, doi: [10.1051/0004-6361/201628867](https://doi.org/10.1051/0004-6361/201628867)
- van der Walt, S., Colbert, S. C., & Varoquaux, G. 2011, Computing in Science Engineering, 13, 22, doi: [10.1109/MCSE.2011.37](https://doi.org/10.1109/MCSE.2011.37)
- Verbunt, F., & Phinney, E. S. 1995, A&A, 296, 709
- Virtanen, P., Gommers, R., Oliphant, T. E., et al. 2020, Nature Methods, 17, 261, doi: [10.1038/s41592-019-0686-2](https://doi.org/10.1038/s41592-019-0686-2)
- Wang, C., & Ryu, T. 2024, arXiv e-prints, arXiv:2410.10314, doi: [10.48550/arXiv.2410.10314](https://doi.org/10.48550/arXiv.2410.10314)
- Webbink, R. F. 1984, ApJ, 277, 355, doi: [10.1086/161701](https://doi.org/10.1086/161701)
- Zahn, J. P. 1977, A&A, 57, 383
- Zhu, J.-P., Liu, L.-D., Yu, Y.-W., et al. 2024, ApJL, 970, L42, doi: [10.3847/2041-8213/ad63a8](https://doi.org/10.3847/2041-8213/ad63a8)
- Ziółkowski, J., & Zdziarski, A. A. 2018, MNRAS, 480, 1580, doi: [10.1093/mnras/sty1948](https://doi.org/10.1093/mnras/sty1948)

## APPENDIX

## A. SUPPLEMENTARY MATERIAL

To obtain realistic initial conditions for our eMT simulations with binaries hosting a BH or NS, we take properties from a POSYDON BPS of systems which initiate MT in a nominally eccentric orbit ( $e > 0.05$ ). In Figure A1, we show this binary population in black, while the samples used for running our f-eMT MESA simulations are shown in orange with Poisson error bars. Error bars on the astrophysical population would be too smaller than the line width. The binary evolution physics prior to oRLO (MT, SN, common envelope evolution, tides) will impact the inferred distribution of binaries which initiate eMT. Other uncertainties in binary evolution, such as the birth eccentricity distribution of MS binaries and the initial mass function will also impact this population.

In our f-eMT simulations, we find a population of binaries which naturally circularize during eMT. We then compare these systems to MESA simulations run with the instantly circularized configuration Section 2.5. The data in Table A1 summarize the MT outcomes of our simulations, comparing the f-eMT models with the instantly circularized ones.

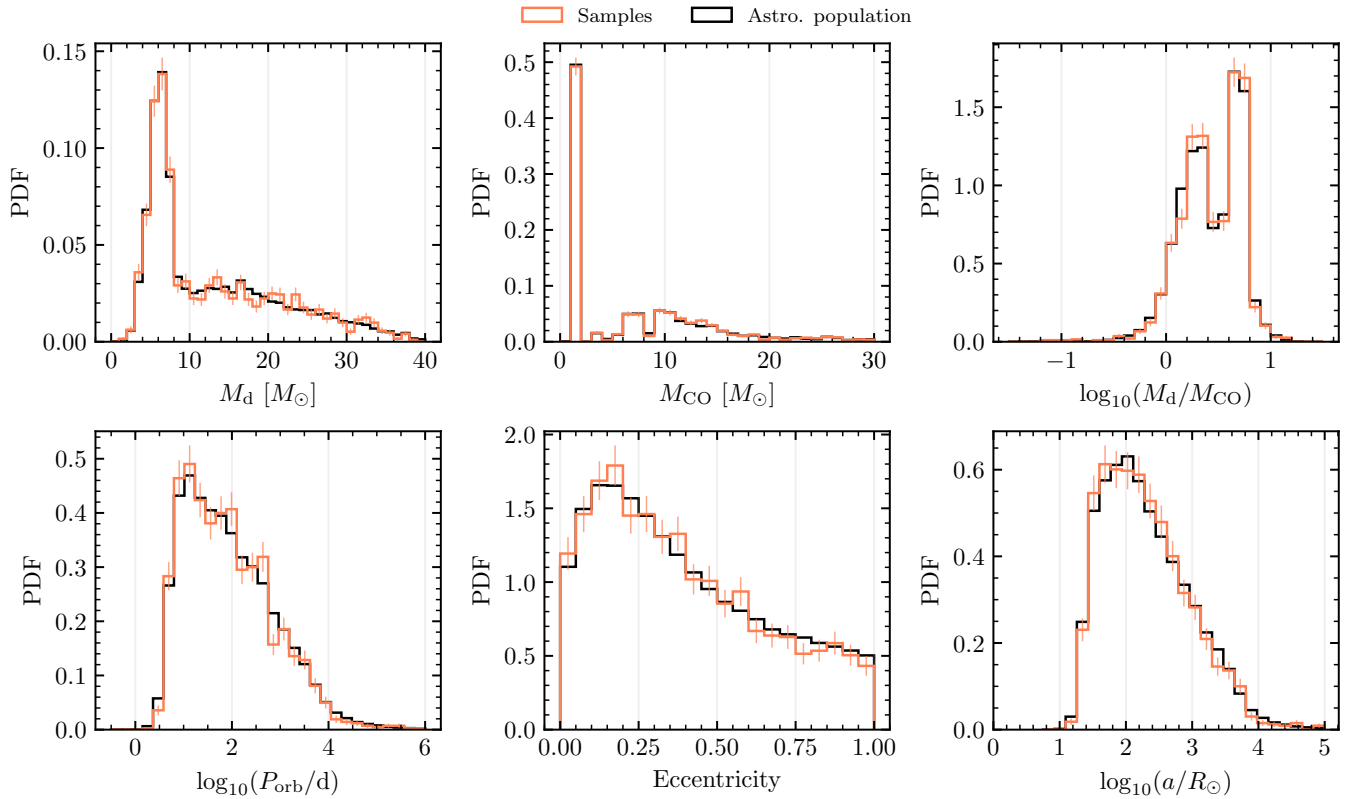


**Figure A1.** One-dimensional distributions of binary parameters from our POSYDON binary population synthesis at the moment a non-degenerate donor star initiates RLO with a BH or NS companion in an eccentric orbit ( $e > 0.05$ ; see Section 2.4.1). The astrophysical binary population (black) is well reproduced by the subset of 2000 samples we simulate with f-eMT in MESA (orange) where vertical lines indicate Poisson errors.



**Table A1.** Mass transfer outcomes for our f-eMT MESA simulations run with the eccentric MT formalism ( $e_i \neq 0$ ), and their associated instantly circularized simulations. This table only shows models which circularize naturally through RLO MT ( $e_f < 0.05$ ), which constitute about 2/3 of all our astrophysically sampled models (see §4.3. For each simulation pair, we show the top three most numerous joint MT cases (reported fractions may not sum to unity). A large fraction (96%) of all models agree in their MT histories, with 4% of models exhibiting completely divergent evolution (i.e. stable vs. unstable MT). For models which agree on the qualitative outcome, they also see good agreement between their detailed MT cases (e.g. both Case B).

| Outcome   | N models  | Eccentric MT ( $e_f < 0.05$ ) | Instantaneous Circ. ( $e_i = 0$ ) | Fraction |
|-----------|-----------|-------------------------------|-----------------------------------|----------|
| Stable MT | 328 (28%) | Case B                        | Case B                            | 52.8%    |
|           |           | Case A/B                      | Case A/B                          | 45.6%    |
|           |           | Case B                        | Case A/B                          | 0.6%     |
| Unstable  | 790 (68%) | Case B                        | Case B                            | 91.9%    |
|           |           | Case A                        | Case A                            | 7.4%     |
|           |           | Case B                        | Case A                            | 0.4%     |
| Mixed TFs | 47 (4%)   | Stable Case B & Case B/BB     | Unstable Case B                   | 64.1%    |
|           |           | Stable Case A/B               | Unstable Case A & Case A/B        | 14.1%    |
|           |           | Unstable Case B               | Stable Case B                     | 12.5%    |